

Measles disease spread and control via vaccination and treatment: A mathematical framework

Zakirullah^{ID}

School of Mathematical Sciences, University of Electronic Science and Technology of China, Chengdu, 611731, China



ARTICLE INFO

Keywords:

Measles mathematical framework
Homotopy Perturbation Method
The Monte Carlo Simulation technique

ABSTRACT

In this paper, we consider a mathematical model for measles. Measles remains a significant concern for global public health, as a single case can lead to the infection of 12 to 18 individuals. Therefore, it is vital to provide control interventions and conceptualize the transmission of measles infection. Parameters of the model are fitted using the nonlinear least squares method. The findings highlight the force of infection rate β as the primary driver behind the variation in measles cases. Furthermore, the analysis revealed that parameter ρ emerged as a key factor contributing to the reduction of measles prevalence. The dynamics of measles are conceptualized with an epidemic model with vaccination and treatment factors. The analysis confirms the existence, uniqueness, and positivity of solutions, provides equilibrium states, and yields the effective reproduction threshold. Moreover, the Bayesian Markov Chain Monte Carlo approach is employed to estimate the model parameters and plot the reproduction threshold. The dynamical behavior of the model is studied through a stability analysis. Using the linearization method, a local stability analysis shows $R_0 < 1$. The Lyapunov functions determine the stability of persistent-infection equilibrium points, ensuring global stability when $R_0 > 1$. Parameter sensitivities were quantified using PRCC, a standard technique in global sensitivity analysis. The model is numerically solved using the Homotopy Perturbation Method.

1. Introduction

Measles is considered a highly transmissible disease affecting populations worldwide, resulting in potentially life-threatening outcomes. In unvaccinated populations, it is more easily transmitted by airborne respiratory droplets. The Paramyxoviridae family includes the measles virus (MeV), an RNA-based pathogen that is characterized by a primary tropism for the respiratory system, ultimately leading to measles. The maculopapular rash on the skin of infected individuals is one of its hallmark clinical features. Infectious diseases like measles remain a significant global public health concern, impacting human and animal populations. The first signs of measles, often similar to flu symptoms, typically manifest around seven to fourteen days following initial exposure to the virus [1–3]. Following the onset of initial measles symptoms, patients typically exhibit the development of red skin rashes within two to five days. Measles usually presents with widespread skin eruptions, which are often preceded or accompanied by Koplik spots, distinctive white lesions found in the oral mucosa. Rashes tend to spread widely throughout the body and manifest with a heightened severity in individuals across all age groups, though infants are particularly vulnerable to serious outcomes [4,5].

Infected individuals transmit the virus mostly through respiratory droplets expelled via coughing or sneezing. Moreover, direct exposure to respiratory secretions, especially in close-proximity settings, significantly influences the rapid transmission of infection [6]. In pregnant women, measles can lead to dangerous effects, leading to premature deliveries and newborns with

E-mail address: zakirullahbzt@gmail.com.

reduced birth weight. Severe complications of measles include brain inflammation (encephalitis), pneumonia, blindness, severe diarrhea with dehydration, ear infections, and serious breathing problems, which can sometimes lead to death. Symptoms of these complications are predominantly found in children below five and individuals over 30, especially malnourished children, individuals with vitamin A deficiencies, and those with weakened immune systems. Measles weakened the immune system, causing the natural defense mechanisms of the body to become impaired, increasing the vulnerability of children to infections. As a result, vaccination prevents the majority of measles-related deaths, highlighting the effectiveness of immunization programs in controlling the spread and reducing its impact [7–9].

In regions where diseases are endemic, vaccination programs have been crucial to protecting individuals. Some vaccines are not fully effective, while others may have side effects or be expensive. In developed countries, intensified immunization campaigns and the availability of affordable, effective, and safe vaccines have significantly reduced measles-related fatalities. The global burden of measles fluctuated significantly between 2000 and 2023. The number of cases reported in 2000 was approximately 28.5 million. A 20% increase from 2022, this number had decreased to 10.3 million cases by 2023 [10]. Despite medical advancements, measles remains a primary cause of death in various areas of Asia and Africa. Several factors contribute to the insufficient vaccination coverage against measles. Misconceptions about vaccines have deterred some individuals from seeking immunization. In rural areas, the availability of healthcare resources is severely constrained, exacerbating the problem, as many miss out on government-organized vaccination programs.

Research shows that low early detection rates. Insufficient health education regarding measles results in its continued transmission. In addition to financial constraints, some patients resort to traditional healing practices over medical care. Global vaccination coverage remains below the WHO (World Health Organization) target despite a reliable and efficient vaccine capable of offering full protection against measles. The first-dose coverage rate is estimated at 85%, markedly lower than the 95% needed to prevent outbreaks, while the second-dose coverage rate is only 67% [11]. Timely administration of both doses is necessary for optimal protection. A highly effective strategy for preventing measles is to vaccinate. Two-dose vaccines are very effective (90%–95%), but in regions like Kenya and sub-Saharan Africa, there is a notable gap in receiving the second dose [12–14]. The eradication of measles remains imperative, necessitating expanded access to vaccinations, the reinforcement of healthcare infrastructure, and targeted interventions to mitigate vaccine hesitancy. Public confidence in vaccines has declined significantly due to the proliferation of misinformation, even within populations that had initially demonstrated willingness. In light of the recent resurgence of measles cases, it is imperative to maintain unwavering vigilance in implementing proactive immunization campaigns [15,16].

Vaccinating all children against measles is significant to ensure protective immunity. In high-risk regions, the first vaccine dose is given at 9 months, followed by the second dose administered according to schedule within a 15 to 18-month range [17]. Combining the vaccine with those for mumps, rubella, and varicella leads to a modest increase in costs, while offering a broader range of protection. Routine vaccination and, in areas with a high incidence of measles, comprehensive immunization programs are vital to reducing the global number of measles-related deaths. The measles vaccine costs less than \$1 per child, which supports its established safety and effectiveness. Furthermore, it is implemented in emergencies to control outbreaks, particularly among vulnerable populations, including refugees. Although it incurs a modestly higher cost, combined vaccines can share delivery expenses and protect against rubella, a common infection that can harm a baby while in utero [18].

Recovery from a measles infection generally results in long-lasting immunity, which offers substantial protection against reinfection in the future [19,20]. Implementing via control and management strategies remains essential, considering the significant health burden and high death rates linked to measles. The clinical approach focuses on alleviating symptoms, maintaining patient comfort and safety, and preventing secondary complications. It is essential to stay properly hydrated, and fluid replacement therapy can be necessary to combat dehydration induced by vomiting or diarrhea. A nutritionally balanced diet plays an important role in promoting recovery. Antibiotic treatment is essential when bacterial infections such as pneumonia or otitis media develop. Moreover, vitamin A supplements are administered to both adults and children within 24 h after diagnosis. Further, this intervention substantially reduces the risk of serious complications, such as blindness and ocular damage, even in those with sufficient diets, by restoring depleted vitamin A levels that can be measured. Similarly, it has been shown that taking vitamin A supplements reduces the overall fatality rate from measles [21].

Modeling approaches offer critical insights into the complexity of disease transmission and progression [22–26]. It can be utilized to assess patterns of transmission and predict the behavior of infectious diseases. Additionally, provide essential insights concerning diseases transmitted and potential epidemic patterns, which are helpful for public health decision-making. These models include demographic characteristics, epidemiological parameters, together with mechanisms of spread to simulate outbreaks. Assess the potential impacts of multiple control measures, predict peak spread rates and predict peak cases [27–30]. Forecasting epidemic patterns, evaluating intervention tactics, and formulating effective public health policies, vaccination campaigns, testing protocols, and lockdowns are enabled by these mathematical frameworks [31–33].

This work builds on the classical SEIR [34] epidemic model to a new SVEITR framework by introducing two additional compartments, vaccination and treatment. The modified model incorporates the combined effects of immunization and recovery interventions, resulting in a reproduction threshold $R_0 = 0.0017$, which signifies strong epidemic control under the estimated parameters. Parameter estimation was conducted using nonlinear least squares with data on WHO-reported measles data [1]. This work also addresses mathematical formulations offering improved analytical stability. In particular, the proposed modified model ensures well-posedness by guaranteeing global existence and boundedness of solutions. Theoretical findings are obtained using the Banach fixed-point theorem and the Picard iterative method to prove the existence, uniqueness, and positivity of solutions, as well as boundedness in the Laplace sense, which strengthens the model of analytical reliability. The threshold behavior and global stability were examined using Lyapunov functions, and parameter influence was quantified through the HPM approach, while sensitivity

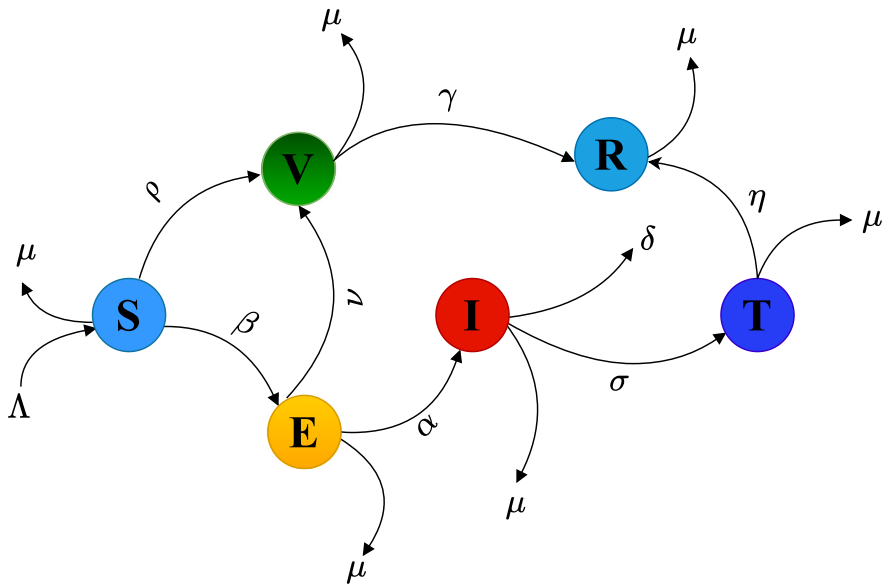


Fig. 1. Schematic of the measles infection dynamics.

analysis identified key parameters that drive transmission. To refine parameter inference, a Bayesian Markov Chain Monte Carlo framework was employed. The impact of four significant parameters was analyzed through the Homotopy Perturbation Method.

The paper proceeds as follows: The first-order mathematical model for measles is formulated in Section 2. NLS estimates parameters in Section 3. Section 4 proves the well-posedness. The computation of equilibria and R_0 is presented in 5. Section 7 analyzes the local and global stability. Section 8 investigates the sensitivity. Section 9 presents the MCMC. Section 10 presents the numerical scheme of the Homotopy Perturbation Method. Section 11 presents numerical simulations and discussions. The final Section 12 concludes the study.

2. Model modification

Here is a description of the measles model, in which N_h is divided into six compartments: susceptible individuals (S), vaccinated individuals (V), exposed individuals (E), infected individuals (I), treatment individuals (T), and recovered individuals (R), based on various epidemiological parameters. The influx of individuals into a susceptible population is denoted by Λ , where μ represents the natural death rate and δ signifies the disease-induced death rate. Susceptible individuals transition to the exposed class through infection, caused by the force of infection rate β , which depends on the interactions between susceptible and infected individuals. Let ρ denote the vaccination rate of susceptible individuals and ν represent the vaccination rate of exposed individuals. Exposed individuals progress to the infected class at a rate of α . Infected individuals undergo treatment, represented by the parameter σ . Treated individuals progress to the recovered category at a recovery rate η , may still contribute to disease transmission before full recovery. Furthermore, vaccinated individuals recover and join the recovered class at a transition rate γ , indicating the effectiveness of vaccination. Below is the flow diagram representing the model structure and parameter interactions.

Using the parameter definitions provided above, together with the flow diagram in Fig. 1, represents the integer measles as ODEs. The system is described by:

$$\begin{aligned}
 \frac{dS}{dt} &= \Lambda - \beta SI - (\mu + \rho)S, \\
 \frac{dV}{dt} &= \rho S + \nu E - (\gamma + \mu)V, \\
 \frac{dE}{dt} &= \beta SI - (\mu + \alpha + \nu)E, \\
 \frac{dI}{dt} &= \alpha E - (\mu + \delta + \sigma)I, \\
 \frac{dT}{dt} &= \sigma I - (\eta + \mu)T, \\
 \frac{dR}{dt} &= \eta T + \gamma V - \mu R,
 \end{aligned} \tag{1}$$

under the initial parameter settings

$$S > 0, V \geq 0, E \geq 0, I \geq 0, T \geq 0, R \geq 0.$$

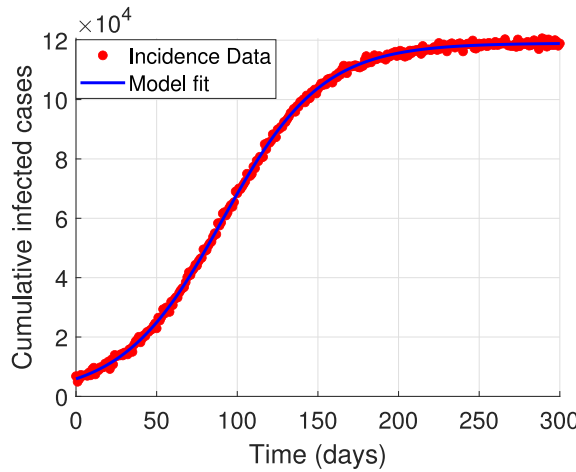


Fig. 2. Cumulative measles cases (red dots) and model fit (blue line).

3. Parameter estimation and data fitting

This section aims to determine the parameters of the mathematical framework (1) based on real-life data from 2023-07 to 2024-06. Model parameter estimation is crucial to providing realistic simulations for predictive analysis and accurately capturing epidemic dynamics. This process minimizes the difference comparing model outputs with the observed data by using a nonlinear least squares method [35–37]. The parameter estimation problem is formulated as the minimization of the sum of squared errors between the model output and the observations, given by:

$$\min_p F(p) = \sum_{i=1}^n [\mathcal{M}(\tau_i, p) - N_{\text{actual}}(\tau_i)]^2 \quad (2)$$

where $\mathcal{M}(\tau_i, p)$ denote the model-predicted number of infected individuals at time τ_i for a given parameter vector p , and $N_{\text{actual}}(\tau_i)$ the corresponding observed number of measles cases. The dataset includes information from 36 countries, obtained from the World Health Organization website [1].

The process involves the following steps:

- The objective function compares values predicted by the model with observed data. The discrepancy between observed and predicted outcomes is quantified using the sum of squared residuals.
- The process of optimization includes altering the parameter values to minimize sum of squared residuals. The optimization process is terminated by convergence criteria, such as a threshold for SSR improvement or a maximum number of iterations.
- Consider that the optimized parameters fail to yield an optimal fit. In that case, the initial guesses are updated and continued until the model predictions closely align with the observed data.

Table 1 presents the estimated parameter values for the measles epidemic model, and **Fig. 2** demonstrates the accuracy of the model in capturing observed dynamics.

4. Well-posedness of the model

The well-posedness of the proposed model (1) is established by proving the existence, uniqueness, positivity, and boundedness of its solutions.

4.1. Existence and uniqueness

This subsection examines the qualitative behavior of the solutions for the measles model described in the system (1) by employing the Banach fixed point theorem. Firstly, the classical integration of both sides of the system (1) results in the following Volterra-type integral equations that lead to

$$\begin{aligned} S(\tau) - S(0) &= \int_0^\tau (\Lambda - \beta S(\tau)I(\tau) - (\mu + \rho)S(\tau))d\tau, \\ V(\tau) - V(0) &= \int_0^\tau (\rho S(\tau) + \nu E(\tau) - (\gamma + \mu)V(\tau))d\tau, \\ E(\tau) - E(0) &= \int_0^\tau (\beta S(\tau)I(\tau) - (\nu + \mu + \alpha)E(\tau))d\tau, \end{aligned} \quad (3)$$

$$\begin{aligned}\mathcal{I}(\tau) - \mathcal{I}(0) &= \int_0^\tau (\alpha\mathcal{E}(\tau) - (\sigma + \mu + \delta)\mathcal{I}(\tau))d\tau, \\ \mathcal{T}(\tau) - \mathcal{T}(0) &= \int_0^\tau (\sigma\mathcal{I}(\tau) - (\eta + \mu)\mathcal{T}(\tau))d\tau, \\ \mathcal{R}(\tau) - \mathcal{R}(0) &= \int_0^\tau (\eta\mathcal{T}(\tau) + \gamma\mathcal{V}(\tau) - \mu\mathcal{R}(\tau))d\tau.\end{aligned}$$

The kernels considered here are defined as:

$$\begin{aligned}Y_1(\tau, S) &= \Lambda - \beta S(\tau)\mathcal{I}(\tau) - (\rho + \mu)S(\tau), \\ Y_2(\tau, \mathcal{V}) &= \rho S(\tau) + \nu\mathcal{E}(\tau) - (\gamma + \mu)\mathcal{V}(\tau), \\ Y_3(\tau, \mathcal{E}) &= \beta S(\tau)\mathcal{I}(\tau) - (\alpha + \nu + \mu)\mathcal{E}(\tau), \\ Y_4(\tau, \mathcal{I}) &= \alpha\mathcal{E}(\tau) - (\delta + \sigma + \mu)\mathcal{I}(\tau), \\ Y_5(\tau, \mathcal{T}) &= \sigma\mathcal{I}(\tau) - (\mu + \eta)\mathcal{T}(\tau), \\ Y_6(\tau, \mathcal{R}) &= \eta\mathcal{T}(\tau) + \gamma\mathcal{V}(\tau) - \mu\mathcal{R}(\tau).\end{aligned}\tag{4}$$

Since $S, \mathcal{V}, \mathcal{E}, \mathcal{I}, \mathcal{T}, \mathcal{R}$ are non-negative bounded functions, there exist positive constants $\phi_i = 1, 2, \dots, 6$ such that $\|S(\tau)\| \leq \phi_1, \|\mathcal{V}(\tau)\| \leq \phi_2, \|\mathcal{E}(\tau)\| \leq \phi_3, \|\mathcal{I}(\tau)\| \leq \phi_4, \|\mathcal{T}(\tau)\| \leq \phi_5, \|\mathcal{R}(\tau)\| \leq \phi_6$.

The notations $\Theta_1 = \rho + \mu + \phi_4\beta, \Theta_2 = \gamma + \mu, \Theta_3 = \mu + \alpha + \nu, \Theta_4 = \mu + \delta + \sigma, \Theta_5 = \eta + \mu, \Theta_6 = \mu$ are also considered. Thus, Eqs. (3) can be equivalently expressed as

$$\begin{aligned}S(\tau) - S(0) &= \int_0^\tau Y_1(t, S(\tau))d\tau, \\ \mathcal{V}(\tau) - \mathcal{V}(0) &= \int_0^\tau Y_1(t, \mathcal{V}(\tau))d\tau, \\ \mathcal{E}(\tau) - \mathcal{E}(0) &= \int_0^\tau Y_1(t, \mathcal{E}(\tau))d\tau, \\ \mathcal{I}(\tau) - \mathcal{I}(0) &= \int_0^\tau Y_1(t, \mathcal{I}(\tau))d\tau, \\ \mathcal{T}(\tau) - \mathcal{T}(0) &= \int_0^\tau Y_1(t, \mathcal{T}(\tau))d\tau \\ \mathcal{R}(\tau) - \mathcal{R}(0) &= \int_0^\tau Y_1(t, \mathcal{R}(\tau))d\tau.\end{aligned}\tag{5}$$

Theorem 4.1. Suppose $0 \leq \Theta_1, \Theta_2, \Theta_3, \Theta_4, \Theta_5, \Theta_6 < 1$, after that, the kernels Y_1, Y_2, Y_3, Y_4, Y_5 and Y_6 meets the Lipschitz condition and are therefore contraction mappings.

Proof. Let Y_1 represent the kernel. If S_1 and S_2 are two arbitrary functions, then it follows that:

$$\begin{aligned}\|Y_1(t, S_1) - Y_1(t, S_2)\| &= \|\Lambda - \beta S_1(\tau)\mathcal{I}(\tau) - (\mu + \rho)S_1(\tau) - (\Lambda - \beta S_2(\tau)\mathcal{I}(\tau) - (\mu + \rho)S_2(\tau))\| \\ &\leq \|(\rho + \mu)S_2(\tau) - (\rho + \mu)S_1(\tau) - \beta\mathcal{I}(\tau)S_1(\tau) + \beta\mathcal{I}(\tau)S_2(\tau)\| \\ &\leq (\rho + \mu + \beta\phi_4) \|S_1(\tau) - S_2(\tau)\| \\ &= \Theta_1 \|S_1(\tau) - S_2(\tau)\|.\end{aligned}\tag{6}$$

Following a similar approach, the results hold for the kernels Y_i , where $i = 2, 3, \dots, 6$.

$$\begin{aligned}\|Y_2(t, \mathcal{V}_1) - Y_2(t, \mathcal{V}_2)\| &= \Theta_2 \|\mathcal{V}_1(\tau) - \mathcal{V}_2(\tau)\|, \\ \|Y_3(t, \mathcal{E}_1) - Y_3(t, \mathcal{E}_2)\| &= \Theta_3 \|\mathcal{E}_1(\tau) - \mathcal{E}_2(\tau)\|, \\ \|Y_4(t, \mathcal{I}_1) - Y_4(t, \mathcal{I}_2)\| &= \Theta_4 \|\mathcal{I}_1(\tau) - \mathcal{I}_2(\tau)\|, \\ \|Y_5(t, \mathcal{T}_1) - Y_5(t, \mathcal{T}_2)\| &= \Theta_5 \|\mathcal{T}_1(\tau) - \mathcal{T}_2(\tau)\|, \\ \|Y_6(t, \mathcal{R}_1) - Y_6(t, \mathcal{R}_2)\| &= \Theta_6 \|\mathcal{R}_1(\tau) - \mathcal{R}_2(\tau)\|.\end{aligned}$$

Thus, the kernels $Y_1, Y_2, Y_3, Y_4, Y_5, Y_6$ satisfy the Lipschitz condition. If $0 \leq \Theta_i < 1$ for $i = 1, 2, \dots, 6$, then $Y_1, Y_2, Y_3, Y_4, Y_5, Y_6$ are contraction mappings which proves the theorem.

In the recursive formulas given by Eqs. (5), the differences between two consecutive terms are as follows:

$$\begin{aligned}\varpi_n(\tau) &= S_n(\tau) - S_{n-1}(\tau) = \int_0^\tau (Y_1(t, S_{n-1}) - Y_1(t, S_{n-2}))d\tau, \\ \kappa_n(\tau) &= \mathcal{V}_n(\tau) - \mathcal{V}_{n-1}(\tau) = \int_0^\tau (Y_2(t, \mathcal{V}_{n-1}) - Y_2(t, \mathcal{V}_{n-2}))d\tau,\end{aligned}$$

$$\begin{aligned}\omega_n(\tau) &= \mathcal{E}_n(\tau) - \mathcal{E}_{n-1}(\tau) = \int_0^\tau (Y_3(t, \mathcal{E}_{n-1}) - Y_3(t, \mathcal{E}_{n-2})) d\tau, \\ \vartheta_n(\tau) &= \mathcal{I}_n(\tau) - \mathcal{I}_{n-1}(\tau) = \int_0^\tau (Y_4(t, \mathcal{I}_{n-1}) - Y_4(t, \mathcal{I}_{n-2})) d\tau, \\ \kappa_n(\tau) &= \mathcal{T}_n(\tau) - \mathcal{T}_{n-1}(\tau) = \int_0^\tau (Y_5(t, \mathcal{T}_{n-1}) - Y_5(t, \mathcal{T}_{n-2})) d\tau, \\ \xi_n(\tau) &= \mathcal{R}_n(\tau) - \mathcal{R}_{n-1}(\tau) = \int_0^\tau (Y_6(t, \mathcal{R}_{n-1}) - Y_6(t, \mathcal{R}_{n-2})) d\tau.\end{aligned}\tag{7}$$

Therefore,

$$\begin{aligned}\varpi_n(\tau) &= \sum_{n=1}^n \mathcal{S}_n(\tau), \quad \varkappa_n(\tau) = \sum_{n=1}^n \mathcal{V}_n(\tau), \quad \omega_n(\tau) = \sum_{n=1}^n \mathcal{E}_n(\tau), \\ \vartheta_n(\tau) &= \sum_{n=1}^n \mathcal{I}_n(\tau), \quad \kappa_n(\tau) = \sum_{n=1}^n \mathcal{T}_n(\tau), \quad \xi_n(\tau) = \sum_{n=1}^n \mathcal{R}_n(\tau).\end{aligned}\tag{8}$$

Applying the norm to both sides of Eqs. (7), and using the Lipschitz condition 4.1 for the kernels, conclude the following inequality:

$$\begin{aligned}\|\varpi_n(\tau)\| &= \|S_n(\tau) - S_{n-1}(\tau)\| = \left\| \int_0^\tau (Y_1(t, S_{n-1}) - Y_1(t, S_{n-2})) d\tau \right\| \\ &\leq \left\| \int_0^\tau (Y_1(t, S_{n-1}) - Y_1(t, S_{n-2})) \right\| d\tau \\ &\leq \Theta_1 t \|S_{n-1} - S_{n-2}\| \\ &= \Theta_1 t \|\varpi_{n-1}(\tau)\| \\ \|\varkappa_n(\tau)\| &= \Theta_2 \|\varkappa_{n-1}(\tau)\| \\ \|\omega_n(\tau)\| &= \Theta_3 \|\omega_{n-1}(\tau)\| \\ \|\vartheta_n(\tau)\| &= \Theta_4 \|\vartheta_{n-1}(\tau)\| \\ \|\kappa_n(\tau)\| &= \Theta_5 \|\kappa_{n-1}(\tau)\| \\ \|\xi_n(\tau)\| &= \Theta_6 \|\xi_{n-1}(\tau)\|.\end{aligned}\tag{9}$$

Based on these findings, we establish the following theorem. \square

Theorem 4.2. *The model for measles has a solution when $\Theta_i \tau_{\max} < 1$, $i = 1, \dots, 6$.*

Proof. Given that $S(\tau), V(\tau), E(\tau), I(\tau), T(\tau)$ and $R(\tau)$ is bounded and Y_1, Y_2, Y_3, Y_4, Y_5 and Y_6 satisfy the Lipschitz condition, the following can be derived from Eqs. (9).

$$\begin{aligned}\|\varpi_n(\tau)\| &\leq \|S_{n-1}(\tau)\| \{\Theta_1 \tau_{\max}\}^n, \quad \|\varkappa_n(\tau)\| \leq \|\mathcal{V}_{n-1}(\tau)\| \{\Theta_2 \tau_{\max}\}^n, \\ \|\omega_n(\tau)\| &\leq \|\mathcal{E}_{n-1}(\tau)\| \{\Theta_3 \tau_{\max}\}^n, \quad \|\vartheta_n(\tau)\| \|\mathcal{I}_{n-1}(\tau)\| \{\Theta_4 \tau_{\max}\}^n, \\ \|\kappa_n(\tau)\| &\leq \|\mathcal{T}_{n-1}(\tau)\| \{\Theta_5 \tau_{\max}\}^n, \quad \|\xi_n(\tau)\| \leq \|\mathcal{R}_{n-1}(\tau)\| \{\Theta_6 \tau_{\max}\}^n.\end{aligned}\tag{10}$$

Using the inequalities from (10) and the fact that the functions defined in (8) exist. The functions $S_n(\tau), V_n(\tau), E_n(\tau), I_n(\tau), T_n(\tau), R_n(\tau)$ approach the solutions of system (1).

Let $C_n^i(\tau), i = 1, \dots, 6$ denote the residual terms following n iterations, corresponding to

$$\begin{aligned}S(\tau) - S(0) &= S_n(\tau) - C_n^1(\tau), \quad V(\tau) - V(0) = V_n(\tau) - C_n^2(\tau), \\ E(\tau) - E(0) &= E_n(\tau) - C_n^3(\tau), \quad I(\tau) - I(0) = I_n(\tau) - C_n^4(\tau), \\ T(\tau) - T(0) &= T_n(\tau) - C_n^5(\tau), \quad R(\tau) - R(0) = R_n(\tau) - C_n^6(\tau).\end{aligned}$$

Applying the Lipschitz condition to Y_1 yields

$$\begin{aligned}\|C_n^1(\tau)\| &= \left\| \int_0^\tau (Y_1(t, S) - Y_1(t, S_{n-1})) d\tau \right\| \leq \Theta_1 t \|S - S_{n-1}\|, \\ &\leq (\Theta_1 t)^2 \|S - S_{n-2}\| \dots (\Theta_1 t)^n \|C_0^1(\tau)\|, \\ &\leq (\Theta_1 t)^n \|S(\tau)\| \leq (\Theta_1 t)^n \phi_1.\end{aligned}$$

Considering the last inequalities at the τ_{\max} point, it follows that

$$\|C_n^1(\tau)\| \leq (\Theta_1 \tau_{\max})^n \phi_1. \tag{11}$$

Taking the limit as $n \rightarrow \infty$, of both sides of the last inequalities and considering Theorem 4.1, obtains $\|C_n^1(\tau)\| \rightarrow 0$. Hence, $\lim_{n \rightarrow \infty} S_n(\tau) = S(\tau) - S(0)$. Similarly, the inequalities for $\|C_n^2(\tau)\|, \|C_n^3(\tau)\|, \|C_n^4(\tau)\|, \|C_n^5(\tau)\|, \|C_n^6(\tau)\|$ can be calculated in the same way. This proves the existence of the solutions for system (1). \square

Theorem 4.3. *The solution of the measles model is unique.*

Proof. Consider $\mathcal{Y}(\tau)$ and $\mathcal{Y}^1(\tau)$ as the solution sets to model:

$$\begin{aligned}\mathcal{Y}(\tau) &= (S(\tau), \mathcal{V}(\tau), \mathcal{E}(\tau), \mathcal{I}(\tau), \mathcal{T}(\tau), \mathcal{R}(\tau)), \\ \mathcal{Y}^1(\tau) &= (S^1(\tau), \mathcal{V}^1(\tau), \mathcal{E}^1(\tau), \mathcal{I}^1(\tau), \mathcal{T}^1(\tau), \mathcal{R}^1(\tau)).\end{aligned}\quad (12)$$

Taking $0 < \Theta_1 t < 1$, into consideration,

$$\left\| S(\tau) - S^1(\tau) \right\| = \left\| \int_0^\tau (Y_1(t, S(\tau)) - Y_1(t, S_{n-1}(\tau))) d\tau \right\| \leq \Theta_1 t \left\| S(\tau) - S^1(\tau) \right\|. \quad (13)$$

Thus, $(1 - \Theta_1 t) \left\| S(\tau) - S^1(\tau) \right\| \leq 0$. Consequently, all compartments in system (1) satisfy $\chi(\tau) = \chi^1(\tau)$, where $\chi(\tau) = (S, \mathcal{V}, \mathcal{E}, \mathcal{I}, \mathcal{T}, \mathcal{R})$, thereby establishing the uniqueness of the solution. \square

4.2. Positivity and boundedness

The solutions of system (1) remain positive and are confined within a biologically feasible region.

Theorem 4.4. *Let*

$$\Omega^+ = \left\{ (S, \mathcal{V}, \mathcal{E}, \mathcal{I}, \mathcal{T}, \mathcal{R}) \in \mathbb{R}_{\geq 0}^6 \mid S > 0, \mathcal{V} \geq 0, \mathcal{E} \geq 0, \mathcal{I} \geq 0, \mathcal{T} \geq 0, \mathcal{R} \geq 0 \right\}.$$

Then, the set Ω^+ is positively invariant under the flow induced by system (1).

Proof. Consider a solution of system (1) starting from an initial condition in Ω^+ .

Using the initial equation of system (1)

$$\frac{dS}{d\tau} = \Lambda - \beta SI - (\mu + \rho)S. \quad (14)$$

Neglecting the infection term $-\beta SI$, we have

$$\frac{dS}{d\tau} \geq \Lambda - (\mu + \rho)S. \quad (15)$$

Applying the Laplace transform yields the following expression:

$$s\mathcal{L}(S) - S(0) \geq \frac{\Lambda}{s} - (\mu + \rho)\mathcal{L}(S). \quad (16)$$

which leads to

$$\mathcal{L}(S) \geq \frac{S(0)}{(s + \rho + \mu)} + \frac{\Lambda}{s(s + \rho + \mu)}. \quad (17)$$

The Inverse Laplace Transform yields

$$S(\tau) \geq S(0)e^{-\tau(\rho+\mu)} + \frac{\Lambda}{\rho + \mu}(1 - e^{-\tau(\rho+\mu)}), \quad \forall t \geq 0. \quad (18)$$

Hence, in the limit as $t \rightarrow \infty$ shows that $S(\tau) > 0$. Applying similar steps to the remaining equations gives

$$\mathcal{V}(\tau) > 0, \quad \mathcal{E}(\tau) \geq 0, \quad \mathcal{I}(\tau) \geq 0, \quad \mathcal{T}(\tau) > 0, \quad \mathcal{R}(\tau) \geq 0, \quad \forall \tau \geq 0. \quad (19)$$

Thus, all solutions starting in Ω^+ remain in Ω^+ , proving positive invariance. \square

Theorem 4.5. *Let*

$$\mathcal{N}(\tau) = S(\tau) + \mathcal{V}(\tau) + \mathcal{E}(\tau) + \mathcal{I}(\tau) + \mathcal{T}(\tau) + \mathcal{R}(\tau).$$

Define the feasible region as

$$\Omega = \left\{ (S, \mathcal{V}, \mathcal{E}, \mathcal{I}, \mathcal{T}, \mathcal{R}) \in \mathbb{R}_{\geq 0}^6 \mid 0 \leq \mathcal{N}(\tau) \leq \mathcal{N}_h \right\}, \quad \mathcal{N}_h = \frac{\Lambda}{\mu}.$$

All solutions that begin within Ω remain within this biologically meaningful domain for all $\tau \geq 0$.

Proof. Summing all compartments of system (1), we obtain

$$\frac{d\mathcal{N}}{d\tau} = \Lambda - \mu\mathcal{N}. \quad (20)$$

Utilizing the Laplace transform, Eq. (20) is simplified to yield

$$s\mathcal{L}(\mathcal{N}) - \mathcal{N}(0) = \frac{\Lambda}{s} - \mu\mathcal{L}(\mathcal{N}), \quad (21)$$

$$\mathcal{L}(\mathcal{N}) = \frac{\mathcal{N}(0)}{(s + \mu)} + \frac{\Lambda}{s(s + \mu)}.$$

The inverse Laplace transform leads to the following form

$$\mathcal{N}(\tau) = \frac{\Lambda}{\mu} + (\mathcal{N}(0) - \frac{\Lambda}{\mu})e^{-\tau\mu}. \quad (22)$$

By letting $\tau \rightarrow \infty$,

$$N(\infty) \leq \frac{\Lambda}{\mu}. \quad (23)$$

Thus, the solutions remain nonnegative and bounded, and the feasible region

$$\Omega = \left\{ (S, V, E, I, T, R) \in \mathbb{R}_{\geq 0}^6 : 0 \leq \mathcal{N}_h(t) \leq \frac{\Lambda}{\mu} \right\}$$

is positively invariant. \square

5. Equilibria and threshold reproduction

This subsection presents the derivation of analyzing the disease-free state, the persistent-infection equilibrium, and the threshold reproduction (R_0).

5.1. Equilibria

The system (1) exhibits two types of steady states: an infection-free equilibrium, where the population is disease-free, and a persistent-infection equilibrium, the pathogen remains at a constant level within the population.

Theorem 5.1. *The system (1) admits a unique infection-free equilibrium point for $R_0 < 1$ and a unique persistent-infection equilibrium point for $R_0 > 1$.*

Proof. To compute the infection-free equilibrium point, we set all infected and exposed compartments equal to zero:

$$\frac{dS}{d\tau} = \frac{dV}{d\tau} = \frac{dE}{d\tau} = \frac{dI}{d\tau} = \frac{dT}{d\tau} = \frac{dR}{d\tau} = 0 \quad (24)$$

Solving (24) gives the infection-free equilibrium point, denoted $E_0 = (S_0, V_0, E_0, I_0, T_0, R_0)$, for which the following expressions hold:

$$E_0 = \left(\frac{\Lambda}{\rho + \mu}, \frac{\rho\Lambda}{(\rho + \mu)(\mu + \gamma)}, 0, 0, 0, 0 \right) \quad (25)$$

We now proceed to derive the persistent-infection equilibrium point, where all compartments are nonzero:

$$\frac{dS}{d\tau} \neq \frac{dV}{d\tau} \neq \frac{dE}{d\tau} \neq \frac{dI}{d\tau} \neq \frac{dT}{d\tau} \neq \frac{dR}{d\tau} \neq 0 \quad (26)$$

The persistent-infection equilibrium point is calculated using back substitution, yielding $E^* = (S^*, V^*, E^*, I^*, T^*, R^*)$, with the components given by:

$$\begin{aligned} S^* &= \frac{(\mu + \alpha + \nu)(\mu + \delta + \sigma)}{\alpha\beta}, \\ V^* &= \frac{(\rho\mu + \nu\mu + \rho\alpha + 2\rho\nu)(\mu + \delta + \sigma)(R_0 - 1)}{\alpha\beta(\gamma + \mu)}, \\ E^* &= \frac{(\mu + \sigma + \delta)(\rho + \mu)(R_0 - 1)}{\alpha\beta}, \\ I^* &= \frac{(\rho + \mu)(R_0 - 1)}{\beta}, \\ T^* &= \frac{\sigma(\rho + \mu)(R_0 - 1)}{\beta(\mu + \eta)}, \\ R^* &= \frac{\sigma\eta\gamma(\rho + \mu)(\rho\mu + \nu\mu + \rho\alpha + 2\rho\nu)(\mu + \delta + \sigma)}{\beta\mu(\mu + \eta)\alpha\beta\mu(\gamma + \mu)}(R_0 - 1). \end{aligned} \quad (27)$$

Here, $S^*, V^*, E^*, I^*, T^*, R^* > 0$, ensuring the existence of a biologically feasible persistent-infection equilibrium point. \square

6. Reproduction threshold (R_0)

In epidemiological modeling, R_0 denotes the average count of new infections caused by a single infectious person when the entire population is susceptible.

Theorem 6.1. For the dynamical system described in model (1), the reproduction threshold R_0 is calculated using the next-generation matrix approach and is expressed as $R_0 = \frac{\Lambda\alpha\beta}{(\rho+\mu)(\delta+\sigma+\mu)(\alpha+\nu+\mu)}$.

Proof. Let $x = (\mathcal{E}, \mathcal{I}, \mathcal{T})$. The dynamics of the model (1) can then be expressed as

$$\frac{dx}{d\tau} = \mathcal{F}(x) - \mathcal{V}(x). \quad (28)$$

To compute the R_0 , we apply the approach [38]. The matrix \mathcal{F} represents new infections arising from contact between susceptible and infectious individuals, while the transition matrix \mathcal{V} is defined as:

$$\mathcal{F}(x) = \begin{pmatrix} \beta S \mathcal{I} \\ 0 \\ 0 \end{pmatrix}, \mathcal{V}(x) = \begin{pmatrix} (\mu + \alpha + \nu)\mathcal{E} \\ -\alpha\mathcal{E} + (\mu + \delta + \sigma)\mathcal{I} \\ -\sigma\mathcal{I} + (\eta + \mu)\mathcal{T} \end{pmatrix}. \quad (29)$$

The partial derivative of Eq. (29) in terms of \mathcal{E} , \mathcal{I} and \mathcal{T} takes the form:

$$\mathcal{F} = \begin{pmatrix} 0 & \beta S_0 & 0 \\ 0 & 0 & 0 \\ 0 & 0 & 0 \end{pmatrix}, \mathcal{V} = \begin{pmatrix} \mu + \alpha + \nu & 0 & 0 \\ -\alpha & \mu + \delta + \sigma & 0 \\ 0 & -\sigma & \eta + \mu \end{pmatrix}. \quad (30)$$

The inverse of \mathcal{V} is,

$$\mathcal{V}^{-1} = \begin{pmatrix} \frac{1}{\alpha+\nu+\mu} & 0 & 0 \\ \frac{\alpha(\eta+\mu)}{(\eta+\mu)(\delta+\sigma+\mu)(\alpha+\nu+\mu)} & \frac{1}{\delta+\sigma_2+\mu} & 0 \\ \frac{\alpha\sigma}{(\eta+\mu)(\delta+\sigma_2+\mu)(\alpha+\nu+\mu)} & \frac{\sigma}{(\eta+\mu)(\delta+\sigma+\mu)} & \frac{1}{\eta+\mu} \end{pmatrix}. \quad (31)$$

After computation using Mathematica, the product matrix $\mathcal{F}\mathcal{V}^{-1}$ gives

$$\mathcal{F}\mathcal{V}^{-1} = \begin{pmatrix} \frac{\Lambda\alpha\beta(\eta+\mu)}{(\rho+\mu)(\eta+\mu)(\delta+\sigma+\mu)(\alpha+\nu+\mu)} & \frac{\Lambda\beta}{(\rho+\mu)(\delta+\sigma+\mu)} & 0 \\ 0 & 0 & 0 \\ 0 & 0 & 0 \end{pmatrix}.$$

The eigenvalue spectrum of $\mathcal{F}\mathcal{V}^{-1}$ are given as

$$\left\{ 0, 0, \frac{\Lambda\alpha\beta}{(\rho + \mu)(\delta + \sigma + \mu)(\alpha + \nu + \mu)} \right\}$$

By taking the spectral radius of $\mathcal{F}\mathcal{V}^{-1}$, the positive eigenvalue represents R_0 as follows:

$$R_0 = \frac{\Lambda\alpha\beta}{(\rho + \mu)(\delta + \sigma + \mu)(\alpha + \nu + \mu)}. \quad \square \quad (32)$$

7. Local and global stability

This section describes local and global stability analysis.

Theorem 7.1. The infection-free equilibrium E_0 is locally stable for $R_0 < 1$ and unstable for $R_0 > 1$.

Proof. Local stability of E_0 follows from the Jacobian eigenvalues:

$$\mathcal{J}_{E_0} = \begin{pmatrix} -(\mu + \rho + \beta\mathcal{I}_0) & 0 & 0 & -\beta S_0 & 0 & 0 \\ \rho & -(\gamma + \mu) & \nu & 0 & 0 & 0 \\ \beta\mathcal{I}_0 & 0 & -(\mu + \alpha + \nu) & \beta S_0 & 0 & 0 \\ 0 & 0 & \alpha & -(\mu + \delta + \sigma) & 0 & 0 \\ 0 & 0 & 0 & \sigma & -(\eta + \mu) & 0 \\ 0 & \gamma & 0 & 0 & \eta & -\mu \end{pmatrix}$$

Evaluated at infection-free equilibrium point, where $\mathcal{I} = \mathcal{E} = 0$:

$$|\mathcal{J}(E_0) - \lambda I| = \begin{vmatrix} -(\mu + \rho) - \lambda & 0 & 0 & -\beta S_0 & 0 & 0 \\ \rho & -(\gamma + \mu) - \lambda & \nu & 0 & 0 & 0 \\ 0 & 0 & -(\mu + \alpha + \nu) - \lambda & \beta S_0 & 0 & 0 \\ 0 & 0 & \alpha & -(\mu + \delta + \sigma) - \lambda & 0 & 0 \\ 0 & 0 & 0 & \sigma & -(\eta + \mu) - \lambda & 0 \\ 0 & \gamma & 0 & 0 & \eta & -\mu - \lambda \end{vmatrix} = 0 \quad (33)$$

The eigenvalues of the Jacobian matrix (33) are

$$\begin{aligned}\lambda_1 &= -\mu - \eta, \\ \lambda_2 &= -\mu, \\ \lambda_3 &= -\gamma - \mu, \\ \lambda_4 &= -\mu - \rho, \\ \lambda_5 &= -\frac{1}{2}(\alpha + \sigma + 2\mu + \delta + \nu) + \frac{1}{2}\sqrt{(\alpha - \sigma - \delta + \nu)^2 + 4\beta S_0 \alpha}, \\ \lambda_6 &= -\frac{1}{2}(\alpha + \sigma + 2\mu + \delta + \nu) - \frac{1}{2}\sqrt{(\alpha - \sigma - \delta + \nu)^2 + 4\beta S_0 \alpha}.\end{aligned}\tag{34}$$

The infection-free equilibrium point of model (1) is locally asymptotically stable if $R_0 < 1$. As five eigenvalues of (34) are strictly negative and the remaining one possess negative real parts, thereby fulfilling the Routh–Hurwitz stability criterion. \square

Theorem 7.2. *The persistent-infection equilibrium E^* is globally stable for $R_0 > 1$ and unstable for $R_0 < 1$.*

Proof. The Lyapunov function takes the following form:

$$\begin{aligned}L(S, V, E, I, R, T) &= \mathcal{K}_1(S + S^* - S^* \ln \frac{S}{S^*}) + \mathcal{K}_2(V + V^* - V^* \ln \frac{V}{V^*}) + \mathcal{K}_3(E + E^* - E^* \ln \frac{E}{E^*}) \\ &\quad + \mathcal{K}_4(I + I^* - I^* \ln \frac{I}{I^*}) + \mathcal{K}_5(T + T^* - T^* \ln \frac{T}{T^*}) + \mathcal{K}_6(R + R^* - R^* \ln \frac{R}{R^*}).\end{aligned}\tag{35}$$

By differentiating Eq. (35) with respect to τ , we obtain:

$$\begin{aligned}\frac{dL}{d\tau} &= \mathcal{K}_1(1 - \frac{S^*}{S})\frac{dS}{d\tau} + \mathcal{K}_2(1 - \frac{V^*}{V})\frac{dV}{d\tau} + \mathcal{K}_3(1 - \frac{E^*}{E})\frac{dE}{d\tau} + \mathcal{K}_4(1 - \frac{I^*}{I})\frac{dI}{d\tau} \\ &\quad + \mathcal{K}_5(1 - \frac{T^*}{T})\frac{dT}{d\tau} + \mathcal{K}_6(1 - \frac{R^*}{R})\frac{dR}{d\tau}.\end{aligned}\tag{36}$$

Substituting the derivatives in system (1) into Eq. (36) leads to:

$$\begin{aligned}\frac{dL}{d\tau} &= \mathcal{K}_1(1 - \frac{S^*}{S})(\Lambda - \beta SI - (\mu + \rho)S) + \mathcal{K}_2(1 - \frac{V^*}{V})(\rho S + vE - (\gamma + \mu)V) \\ &\quad + \mathcal{K}_3(1 - \frac{E^*}{E})(\beta SI - (\mu + \alpha + \nu)E) + \mathcal{K}_4(1 - \frac{I^*}{I})(\alpha E - (\mu + \delta + \sigma)I) \\ &\quad + \mathcal{K}_5(1 - \frac{T^*}{T})(\sigma I - (\eta + \mu)T) + \mathcal{K}_6(1 - \frac{R^*}{R})(\eta T + \gamma V - \mu R).\end{aligned}\tag{37}$$

Substituting Eq. (27) into Eq. (37) leads to:

$$\begin{aligned}\frac{dL}{d\tau} &= \mathcal{K}_1\beta S^* I^* \left(1 + \frac{I}{I^*} - \frac{S^*}{S} - \frac{SI}{S^* I^*}\right) - \mathcal{K}_1(\mu + \rho)S^* \left(\frac{S}{S^*} - \frac{S^*}{S}\right) + \mathcal{K}_2\rho S^* \left(1 + \frac{S}{S^*} - \frac{V}{V^*} - \frac{SV^*}{S^* V}\right) \\ &\quad + vE^* \mathcal{K}_2 \left(1 + \frac{E}{E^*} - \frac{V}{V^*} - \frac{V^* E}{V^* E^*}\right) + \mathcal{K}_3\beta S^* I^* \left(1 + \frac{S}{S^*} \frac{I}{I^*} - \frac{E}{E^*} - \frac{SE^* I}{S^* E^* I^*}\right) + \mathcal{K}_4\alpha E^* \left(1 + \frac{E}{E^*} - \frac{I}{I^*} - \frac{EI^*}{E^* I}\right) \\ &\quad + \mathcal{K}_5\sigma I^* \left(1 + \frac{I}{I^*} - \frac{T}{T^*} - \frac{IT^*}{I^* T}\right) + \mathcal{K}_6\eta T^* \left(1 + \frac{T}{T^*} - \frac{R}{R^*} - \frac{R^* T}{R^* T^*}\right) + \mathcal{K}_6\gamma V^* \left(1 + \frac{V}{V^*} - \frac{R}{R^*} - \frac{VR^*}{V^* R}\right).\end{aligned}\tag{38}$$

Through algebraic manipulation, Eq. (38) reduces to:

$$\begin{aligned}\frac{dL}{d\tau} &= \frac{(vE^* - \rho S^*)(\mu + \rho)}{\rho}(3 - \frac{SV^*}{S^* V} - \frac{V}{V^*} - \frac{S^*}{S}) - \beta I^* S^*(3 - \frac{EI^*}{E^* I} - \frac{SE^* I}{S^* E^* I} - \frac{S^*}{S}) \\ &\quad - \frac{E^*(\mu + \rho)v}{\rho}(4 - \frac{VR^*}{V^* R} - \frac{SV^*}{S^* V} - \frac{R}{R^*} - \frac{S^*}{S})\end{aligned}\tag{39}$$

By the arithmetic–geometric mean inequality, the inequalities in (39) are obtained as:

$$3 - \frac{SV^*}{S^* V} - \frac{V}{V^*} - \frac{S^*}{S} \leq 0.$$

Thus, $\frac{dL}{d\tau} \leq 0$ for $R_0 > 1$, and $\frac{dL}{d\tau} = 0$ at $S = S^*, V = V^*, E = E^*, I = I^*, R = R^*$. LaSalle's invariance principle implies that when $R_0 > 1$, the system approaches the persistent-infection equilibrium in Ω from any initial condition, indicating global asymptotic stability. \square

8. Sensitivity analysis

The sensitivity of R_0 to parameter p_i is measured via the normalized forward index.

$$S_{p_i}^{R_0} = \frac{\partial R_0}{\partial p_i} \cdot \frac{p_i}{R_0}.\tag{40}$$

Table 1

Description of parameters employed in the system.

Parameters	Descriptions	Values	References
μ	Natural death rate	0.004 days^{-1}	Fitted
Λ	Influx rate of individuals into the susceptible	0.500 days^{-1}	[39]
β	Force of infection	0.0019 days^{-1}	Fitted
ρ	Vaccination rate of susceptible	0.0091 days^{-1}	Fitted
α	Progression rate from exposed to infected	0.0256 days^{-1}	Fitted
v	Vaccination rate of exposed	0.0011 days^{-1}	Fitted
δ	Disease-induced death rate	0.1304 days^{-1}	Fitted
σ	Treatment rate of infected individuals	0.0010 days^{-1}	Fitted
γ	Recovery rate of vaccinated	0.8000 days^{-1}	Fitted
η	Recovery rate of treated infected	0.0010 days^{-1}	Fitted

It measures the proportional effect of a change in parameter p_i on R_0 , allowing identification of the key drivers of transmission. The calculation of the sensitivity index for parameters $\Lambda, \beta, \alpha, \mu, \rho, v, \delta$, and σ is as follows:

$$\begin{aligned}\Gamma_{\Lambda}^{R_0} &= \frac{\partial R_0}{\partial \Lambda} \times \frac{\Lambda}{R_0} = 1 > 0, \\ \Gamma_{\beta}^{R_0} &= \frac{\partial R_0}{\partial \beta} \times \frac{\beta}{R_0} = 1 > 0, \\ \Gamma_{\alpha}^{R_0} &= 1 - \frac{\alpha}{(\alpha + v + \mu)} > 0, \\ \Gamma_{\mu}^{R_0} &= 1 - \frac{\mu}{(\alpha + v + \mu)} - \frac{\mu}{(\delta + \sigma_2 + \mu)} - \frac{\mu}{(\rho + \mu)} > 0, \\ \Gamma_{\rho}^{R_0} &= -\frac{\rho}{\rho + \mu} < 0, \\ \Gamma_v^{R_0} &= -\frac{v}{\alpha + v + \mu} < 0, \\ \Gamma_{\delta}^{R_0} &= -\frac{\delta}{\sigma + \delta + \mu} < 0, \\ \Gamma_{\sigma}^{R_0} &= -\frac{\sigma}{\delta + \sigma + \mu} < 0.\end{aligned}$$

Findings from the sensitivity analysis indicate that the model behavior is most responsive to the force of infection (β) and the influx rate of individuals into the susceptible (Λ), both with calculated indices of +1. Therefore, 1% increase in either parameter leads to a proportional 1% increase in disease transmission.

In contrast, the disease-induced death rate ($\delta = -0.96$) significantly reduces transmission; a 1% increase in δ results in 0.96% decrease in the outcome. Vaccination of susceptibles ($\rho = -0.69$) also shows a substantial protective effect, where a 1% increase reduces the disease burden by approximately 0.7%. The natural mortality rate ($\mu = +0.53$) has a slightly positive effect in this approach, implying that a 1% rise in μ increases the outcome by about 0.5%. Transition rate from exposed to infectious individuals ($\alpha = +0.17$) contributes positively but modestly, with a 1% increase raising the outcome by 0.17%.

Vaccination of exposed ($v = -0.04$) and treatment rate of infected ($\sigma = -0.007$) have minimal effects, decreasing the outcome by less than 0.05% and 0.01%, respectively, for a 1% increase. Specifically, controlling transmission (β), limiting susceptible influx (Λ), and strengthening vaccination (ρ) provide the most effective levers for reducing disease burden, whereas other parameters have only slight effects.

9. Markov chain Monte Carlo

The MCMC technique provides a Bayesian framework for estimating parameters of complex dynamical systems [40,41]. These approaches are useful in mathematical modeling of infectious diseases such as measles, where the high-dimensional parameter space and the likelihood function is usually analytically intractable. For each parameter draw, the model was integrated over 300 days and compared with observed data. A total of 10^4 posterior samples were generated for each of the 10 parameters. Adaptive runs were performed to ensure chain stabilization before sampling. Initial values for parameters were obtained via least-squares estimates, and convergence of the MCMC chains determined the identifiability of the model parameters. The R_0 was assessed over 10^4 iterations, with scenarios exhibiting both $R_0 < 1$ and $R_0 > 1$.

The objective function minimized during parameter initialization was defined as

$$SS(\theta) = \sum_{i=1}^n [v_i - g(f(u_i, \theta))]^2, \quad (41)$$

where v_i denotes the observed data, $f(u_i, \theta)$ the model prediction, and θ the vector of model parameters. Minimization of $SS(\theta)$ quantifies the discrepancy between the model and observations.

Linearization around the best-fitting point $\tilde{\theta}$ yields the approximate parameter covariance matrix

$$\text{Cov}(\theta) = \sigma^2(J^\top J)^{-1}, \quad (42)$$

where J is the Jacobian matrix with elements

$$J_{ip} = \frac{\partial g(f(u_i, \tilde{\theta}))}{\partial \theta_p}.$$

Furthermore, autocorrelation times were short, and convergence diagnostics such as Geweke statistics were close to unity. Posterior skewness and kurtosis approximate Gaussian values (0 and 3), which supports the normality of the estimated parameters.

10. Homotopy perturbation method

In 1999, J. He introduced efficient semi-analytical approach (HPM) for differential equations [42]. This approach is an efficient semi-analytical framework for non-linear epidemic dynamics. Without involving linearization, discretization, or perturbative smallest parameters, the method provides systematic series solutions that converge towards the dynamic. This flexibility underscores the broad potential of this approach for the analysis of complex nonlinear problems across disciplines. The method simplifies complex calculations and offers an efficient method for analyzing the dynamics of the variables S, V, E, I, T , and R under different contexts. The convergence of the method has been thoroughly studied in the literature (see [43]). This method constructs a homotopy $\mathcal{H}(v, \mathcal{P})$ and $\mathcal{P} \in [0, 1]$ stands for the embedding parameter. The homotopy formulation is as follows:

$$\mathcal{H}(v, \mathcal{P}) = (1 - \mathcal{P})[\mathcal{L}(v) - \mathcal{L}(u_0)] + \mathcal{P}[\mathcal{L}(v) + \mathcal{N}(v) - f(r)] = 0, \quad (43)$$

where $\mathcal{L}(v)$ and $\mathcal{N}(v)$ stand for the linear and nonlinear operators of the original problem, and u_0 is an initial approximation that satisfies the boundary conditions.

We express the solution v as a series in terms of the parameter \mathcal{P} :

$$v(t; \mathcal{P}) = v_0(t) + \mathcal{P}v_1(t) + \mathcal{P}^2v_2(t) + \dots, \quad (44)$$

leading to the approximate solution

$$u(t) = \lim_{\mathcal{P} \rightarrow 1} v(t; \mathcal{P}). \quad (45)$$

When $\mathcal{P} \rightarrow 1$, this series converges to the solution of the original problem, allowing complex terms to be handled progressively. Subsequently,

$$\begin{aligned} \mathcal{H}(S, \mathcal{P}) &= (1 - \mathcal{P})\left(\frac{dS}{d\tau} - \frac{dS_0}{d\tau}\right) + \mathcal{P}\left(\frac{dS}{d\tau} - \Lambda - \beta SI - (\mu + \rho)S\right) = 0, \\ \mathcal{H}(V, \mathcal{P}) &= (1 - \mathcal{P})\left(\frac{dV}{d\tau} - \frac{dV_0}{d\tau}\right) + \mathcal{P}\left(\frac{dV}{d\tau} - \rho S + \nu E - (\gamma + \mu)V\right) = 0, \\ \mathcal{H}(E, \mathcal{P}) &= (1 - \mathcal{P})\left(\frac{dE}{d\tau} - \frac{dE_0}{d\tau}\right) + \mathcal{P}\left(\frac{dE}{d\tau} - \beta SI - (\mu + \alpha + \nu)E\right) = 0, \\ \mathcal{H}(I, \mathcal{P}) &= (1 - \mathcal{P})\left(\frac{dI}{d\tau} - \frac{dI_0}{d\tau}\right) + \mathcal{P}\left(\frac{dI}{d\tau} - \alpha E - (\mu + \delta + \sigma)I\right) = 0, \\ \mathcal{H}(T, \mathcal{P}) &= (1 - \mathcal{P})\left(\frac{dT}{d\tau} - \frac{dT_0}{d\tau}\right) + \mathcal{P}\left(\frac{dT}{d\tau} - \sigma I - (\eta + \mu)T\right) = 0, \\ \mathcal{H}(R, \mathcal{P}) &= (1 - \mathcal{P})\left(\frac{dR}{d\tau} - \frac{dR_0}{d\tau}\right) + \mathcal{P}\left(\frac{dR}{d\tau} - \eta T + \gamma V - \mu R\right) = 0. \end{aligned} \quad (46)$$

Let the solutions to Eqs. (46) be in the following forms:

$$\begin{aligned} S &= S_0 + S_1\mathcal{P} + S_2\mathcal{P}^2 + S_3\mathcal{P}^3 + S_4\mathcal{P}^4 + S_5\mathcal{P}^5 + S_6\mathcal{P}^6 + \dots, \\ V &= V_0 + V_1\mathcal{P} + V_2\mathcal{P}^2 + V_3\mathcal{P}^3 + V_4\mathcal{P}^4 + V_5\mathcal{P}^5 + V_6\mathcal{P}^6 + \dots, \\ E &= E_0 + E_1\mathcal{P} + E_2\mathcal{P}^2 + E_3\mathcal{P}^3 + E_4\mathcal{P}^4 + E_5\mathcal{P}^5 + E_6\mathcal{P}^6 + \dots, \\ I &= I_0 + I_1\mathcal{P} + I_2\mathcal{P}^2 + I_3\mathcal{P}^3 + I_4\mathcal{P}^4 + I_5\mathcal{P}^5 + I_6\mathcal{P}^6 + \dots, \\ T &= T_0 + T_1\mathcal{P} + T_2\mathcal{P}^2 + T_3\mathcal{P}^3 + T_4\mathcal{P}^4 + T_5\mathcal{P}^5 + T_6\mathcal{P}^6 + \dots, \\ R &= R_0 + R_1\mathcal{P} + R_2\mathcal{P}^2 + R_3\mathcal{P}^3 + R_4\mathcal{P}^4 + R_5\mathcal{P}^5 + R_6\mathcal{P}^6 + \dots \end{aligned}$$

Therefore:

$$\mathcal{H}(S, \mathcal{P}) = (1 - \mathcal{P})\left(\sum_{i=0}^{\infty} \mathcal{P}^i \frac{dS_i}{d\tau} - \frac{dS_0}{d\tau}\right) + \mathcal{P}\left(\sum_{i=0}^{\infty} \mathcal{P}^i \frac{dS_i}{d\tau} - \Lambda - \beta \sum_{i=0}^{\infty} \mathcal{P}^i S_i \sum_{i=0}^{\infty} \mathcal{P}^i I_i - (\mu + \rho) \sum_{i=0}^{\infty} \mathcal{P}^i S_i\right) = 0, \quad (47)$$

$$\mathcal{H}(V, \mathcal{P}) = (1 - \mathcal{P})\left(\sum_{i=0}^{\infty} \mathcal{P}^i \frac{dV_i}{d\tau} - \frac{dV_0}{d\tau}\right) + \mathcal{P}\left(\sum_{i=0}^{\infty} \mathcal{P}^i \frac{dV_i}{d\tau} - \rho \sum_{i=0}^{\infty} \mathcal{P}^i S_i + \nu \sum_{i=0}^{\infty} \mathcal{P}^i E_i - (\gamma + \mu) \sum_{i=0}^{\infty} \mathcal{P}^i V_i\right) = 0, \quad (48)$$

$$\mathcal{H}(E, \mathcal{P}) = (1 - \mathcal{P})\left(\sum_{i=0}^{\infty} \mathcal{P}^i \frac{dE_i}{d\tau} - \frac{dE_0}{d\tau}\right) + \mathcal{P}\left(\sum_{i=0}^{\infty} \mathcal{P}^i \frac{dE_i}{d\tau} - \beta \sum_{i=0}^{\infty} \mathcal{P}^i S_i \sum_{i=0}^{\infty} \mathcal{P}^i I_i - (\mu + \alpha + \nu) \sum_{i=0}^{\infty} \mathcal{P}^i E_i\right) = 0, \quad (49)$$

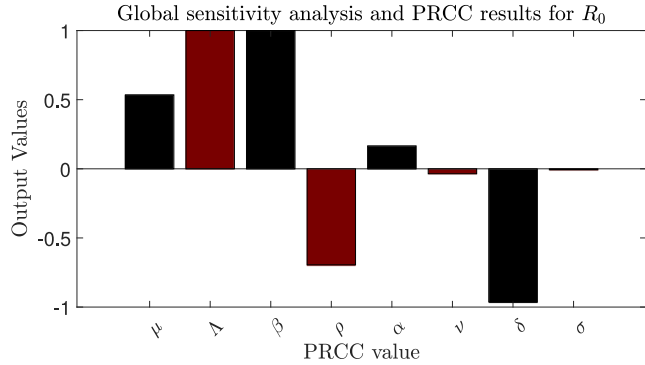


Fig. 3. Evaluation of the relative impact of model parameters on R_0 through sensitivity analysis.

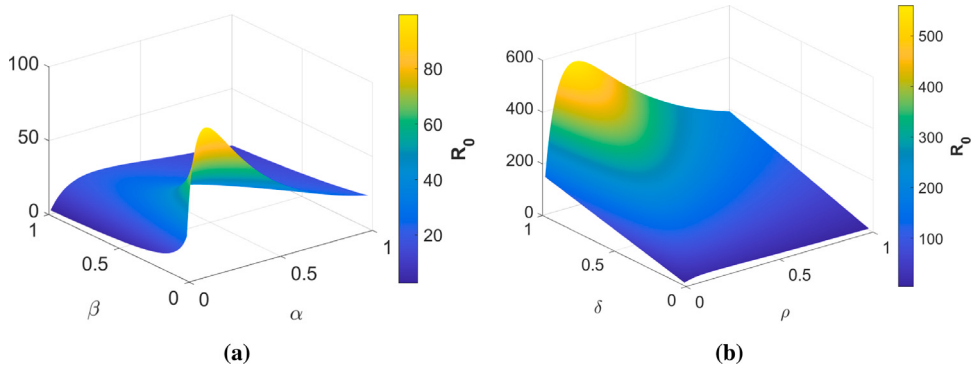


Fig. 4. Three-dimensional surface of R_0 as a function of parameters α , β , ρ and δ .

$$\mathcal{H}(\mathcal{I}, \mathcal{P}) = (1 - \mathcal{P}) \left(\sum_{i=0}^{\infty} \mathcal{P}^i \frac{d\mathcal{I}_i}{d\tau} - \frac{d\mathcal{I}_0}{d\tau} \right) + \mathcal{P} \left(\sum_{i=0}^{\infty} \mathcal{P}^i \frac{d\mathcal{T}_i}{d\tau} - \alpha \sum_{i=0}^{\infty} \mathcal{P}^i \mathcal{E}_i - (\mu + \delta + \sigma) \sum_{i=0}^{\infty} \mathcal{P}^i \mathcal{I}_i \right) = 0, \quad (50)$$

$$\mathcal{H}(\mathcal{T}, \mathcal{P}) = (1 - \mathcal{P}) \left(\sum_{i=0}^{\infty} \mathcal{P}^i \frac{d\mathcal{T}_i}{d\tau} - \frac{d\mathcal{T}_0}{d\tau} \right) + \mathcal{P} \left(\sum_{i=0}^{\infty} \mathcal{P}^i \frac{d\mathcal{R}_i}{d\tau} - \sigma \sum_{i=0}^{\infty} \mathcal{P}^i \mathcal{I}_i - (\eta + \mu) \sum_{i=0}^{\infty} \mathcal{P}^i \mathcal{T}_i \right) = 0, \quad (51)$$

$$\mathcal{H}(\mathcal{R}, \mathcal{P}) = (1 - \mathcal{P}) \left(\sum_{i=0}^{\infty} \mathcal{P}^i \frac{d\mathcal{R}_i}{d\tau} - \frac{d\mathcal{R}_0}{d\tau} \right) + \mathcal{P} \left(\sum_{i=0}^{\infty} \mathcal{P}^i \frac{d\mathcal{V}_i}{d\tau} - \eta \sum_{i=0}^{\infty} \mathcal{P}^i \mathcal{T}_i + \gamma \sum_{i=0}^{\infty} \mathcal{P}^i \mathcal{V}_i - \mu \sum_{i=0}^{\infty} \mathcal{P}^i \mathcal{R}_i \right) = 0. \quad (52)$$

11. Numerical results and discussion

In this section, the significance of the obtained numerical solutions is addressed for our proposed model (1). The system (1) is initialized with the following conditions: $S(0) = 600$, $\mathcal{V}(0) = 500$, $\mathcal{E}(0) = 300$, $\mathcal{I}(0) = 550$, $\mathcal{T}(0) = 100$ and $\mathcal{R}(0) = 100$, with parameter values provided in Table 1.

Fig. 3 illustrates the PRCC output for R_0 , indicating the sensitivity of R_0 to the various model parameters, identifying the most significant parameters in the transmission of measles. The bars represent PRCC outcomes for the considered parameters, illustrating their impact on R_0 . Parameters possessing positive values result in a direct effect, and those with negative values exhibit an inverse impact.

In Fig. 4, demonstrates a connection between the R_0 and critical parameters influencing it, including α , β , δ and ρ . The surface plot illustrates the variation of R_0 with respect to parameters. A shorter latent period is implied by a higher α , which accelerates the transition from exposed to infected and leads to an increase in R_0 . As the infection parameter β increases, more susceptible individuals contract the disease, causing R_0 to rise. Higher δ reduces the number of infected individuals that propagate infection, leading to a decline in R_0 and transmission capacity. Fig. 5 illustrates that vaccination is applied to the exposed population, thereby reducing transition rate to the infectious compartment, which in turn lowers R_0 . Increasing both σ and ν can considerably reduce R_0 . A higher treatment rate shortens the infectious stage duration, thereby reducing the force of infection and decreasing R_0 .

Furthermore, we examined the impact of parameters σ , ρ , ν , and β and varied across different classes in the model (1) employing the HMP approach. Fig. 6 illustrates the effect of increasing the treatment rate σ . The findings demonstrate that higher treatment rates substantially reduced infectivity among hosts over time. In Fig. 7, examine the effect of vaccinating the exposed class, with vaccination rates ρ . In Fig. 8, the vaccination of susceptible individuals, with vaccination rates ν . In both cases, increasing vaccination

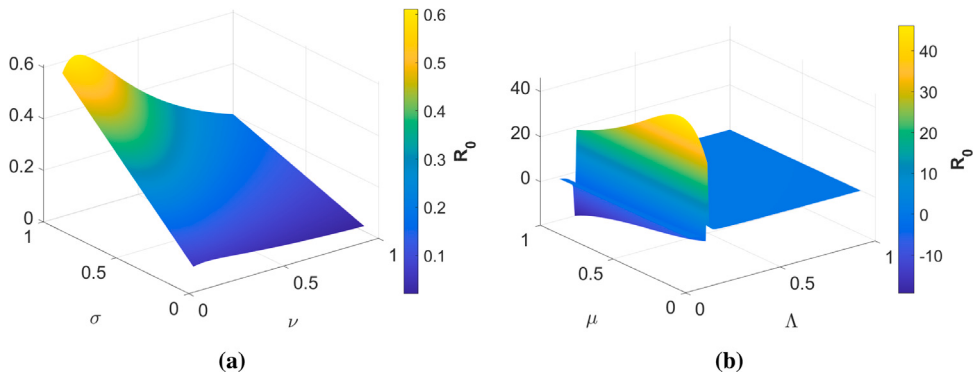


Fig. 5. Three-dimensional surface of R_0 as a function of parameters ν , σ , Λ and μ .

coverage leads to a significant reduction in the transmission dynamics of measles. Notably, in Fig. 9, progressive suppression occurs in the exposed and infectious classes as vaccination rates increase, which illustrates the combined role of early intervention.

Fig. 10(a) shows that the samples with $R_0 < 1$ correspond to controlled transmission conditions, where infection spread declines over time. Fig. 10(b) illustrates that samples with $R_0 > 1$ indicate sustained transmission and potential epidemic growth. Each simulation index represents a posterior realization obtained from the MCMC chain. The distribution of samples across both regimes highlights the model's robustness to capture transitions between subcritical and supercritical epidemic dynamics.

Figs. 11(a)–20(a) illustrate trace plots for the model parameters. Each trace shows stable sampling across 100,000 iterations with no visible drift, confirming stationarity of the MCMC chains. Figs. 11(b)–20(b) display the corresponding posterior densities, which approximate normal distributions centered near their posterior means, indicating well-mixed samples and minimal autocorrelation. Collectively, these diagnostics demonstrate that the MCMC procedure achieved convergence for all parameters, ensuring reliable posterior inference across the model.

In Fig. 21(a), all eigenvalues remain below zero, where $\lambda_i < 0$ for all $i = 1, \dots, 6$, indicating that the infection-free point is locally stable for eigenvalues, signifying that the infection will eventually die out. Fig. 21(b), eigenvalues are positive, where $\lambda_i > 0$ for all $i = 1, \dots, 6$, ensuring the instability that the disease remains present in the population over time.

The phase portrait in Fig. 22 illustrates the equilibrium dynamics of the system (1). Blue and red streamlines represent the normalized vector field of the compartments, indicating the direction of population changes over time. The black filled circle marks the equilibrium point, highlighting the state toward which trajectories converge. This visualization demonstrates that the system is dynamically stable, as trajectories originating from different initial conditions all flow toward the equilibrium.

12. Conclusion

A compartmental model was developed to study the measles transmission in the presence of vaccination and treatment strategies. The NLS method was first employed to obtain initial parameter estimates by minimizing the residuals. The MCMC approach was then applied to refine these estimates within a Bayesian framework, enabling quantification of parameter uncertainty and confirming convergence of the inferred posterior distributions. This combined strategy improved the robustness and reliability of the model calibration process. The next-generation matrix technique was utilized to evaluate the reproduction threshold. Stability analysis confirms that the infection-free equilibrium was locally asymptotically stable when $R_0 < 1$, while a unique persistent infection is globally stable for $R_0 > 1$ via Lyapunov methods. Using PRCC and the sensitivity index formula, we investigated the impact of R_0 on the system through sensitivity analysis. Parameters β showed positive sensitivity indices, significantly affecting measles transmission and prevalence. In contrast, the sensitivity indices of parameters ρ , ν , and δ exhibited negative values significantly mitigating infection spread. The results demonstrate critical parameters for controlling measles infections and evaluate existing vaccination and treatment strategies. Vaccinating the susceptible population can substantially reduce infection prevalence, and eradication is possible with treatment proving effective in reducing the infectious population. Furthermore, enhancing treatment rates contributes to reducing the spread of measles, although it may increase the number of susceptibles while leading to a reduction in the infected population.

Additionally, this work also has several limitations. In this model, homogeneous mixing is assumed, and parameter values are constant. These assumptions may not accurately reflect realistic contact patterns or time-varying intervention intensities. This description of vaccination and treatment processes is simplified, and in real-world implementation, delays, partial immunity, and heterogeneous access may occur. Data used for parameter estimation are aggregated monthly by WHO, limiting temporal resolution and possibly impacting parameter sensitivity. As the model is deterministic, it does not take into account demographic or stochastic fluctuations that may influence outbreak behavior in small populations. In future work, we will consider optimal control strategy, fractional-order dynamics, age structure, interventions with time-varying effects, and stochastic effects.

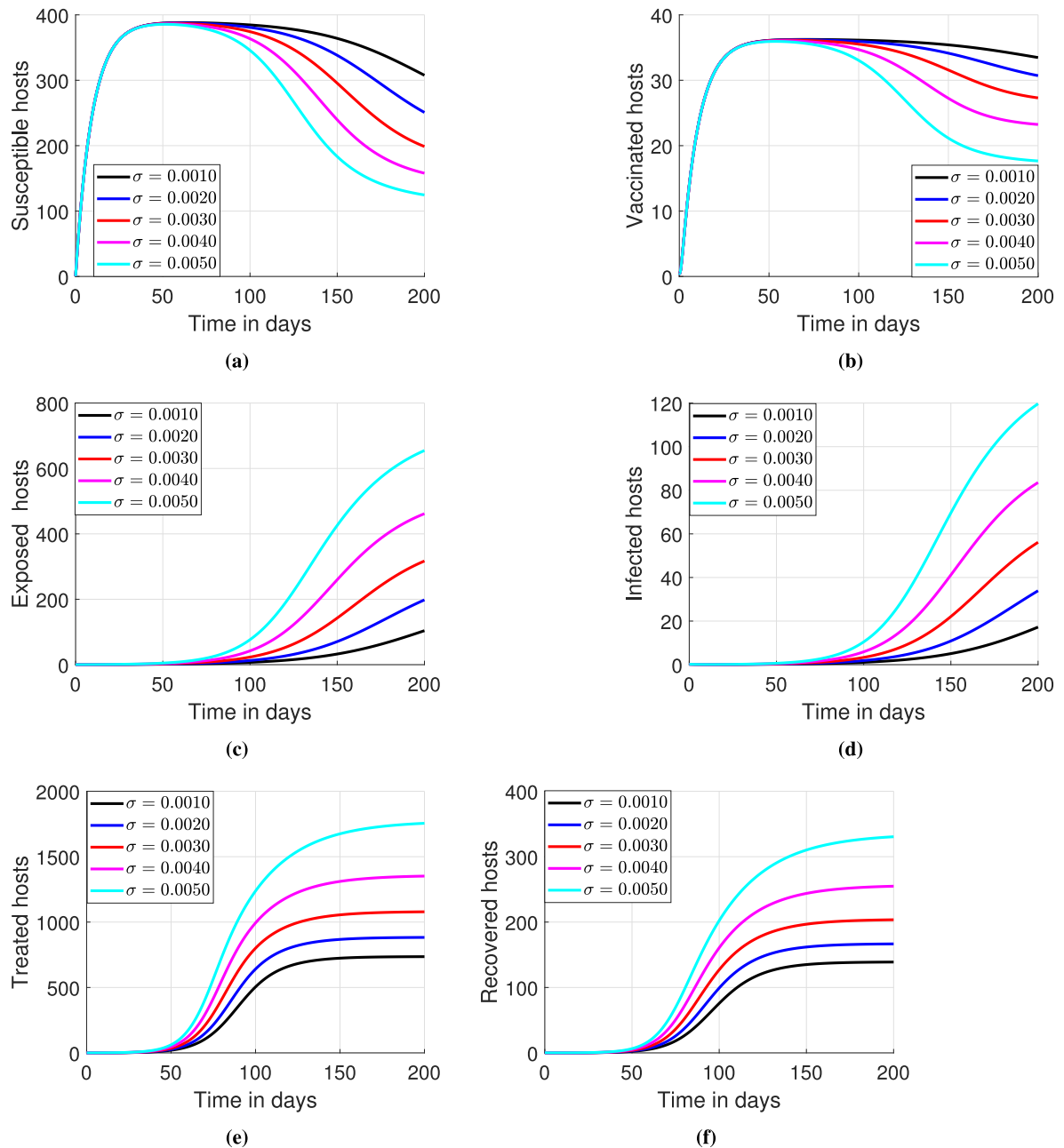


Fig. 6. Dynamics of the *SVETIR* population under varying σ .

Declaration of competing interest

The authors declare that they have no known competing financial interests or personal relationships that could have appeared to influence the work reported in this paper.

Acknowledgments

The author appreciates the referees constructive comments that improved the manuscript.

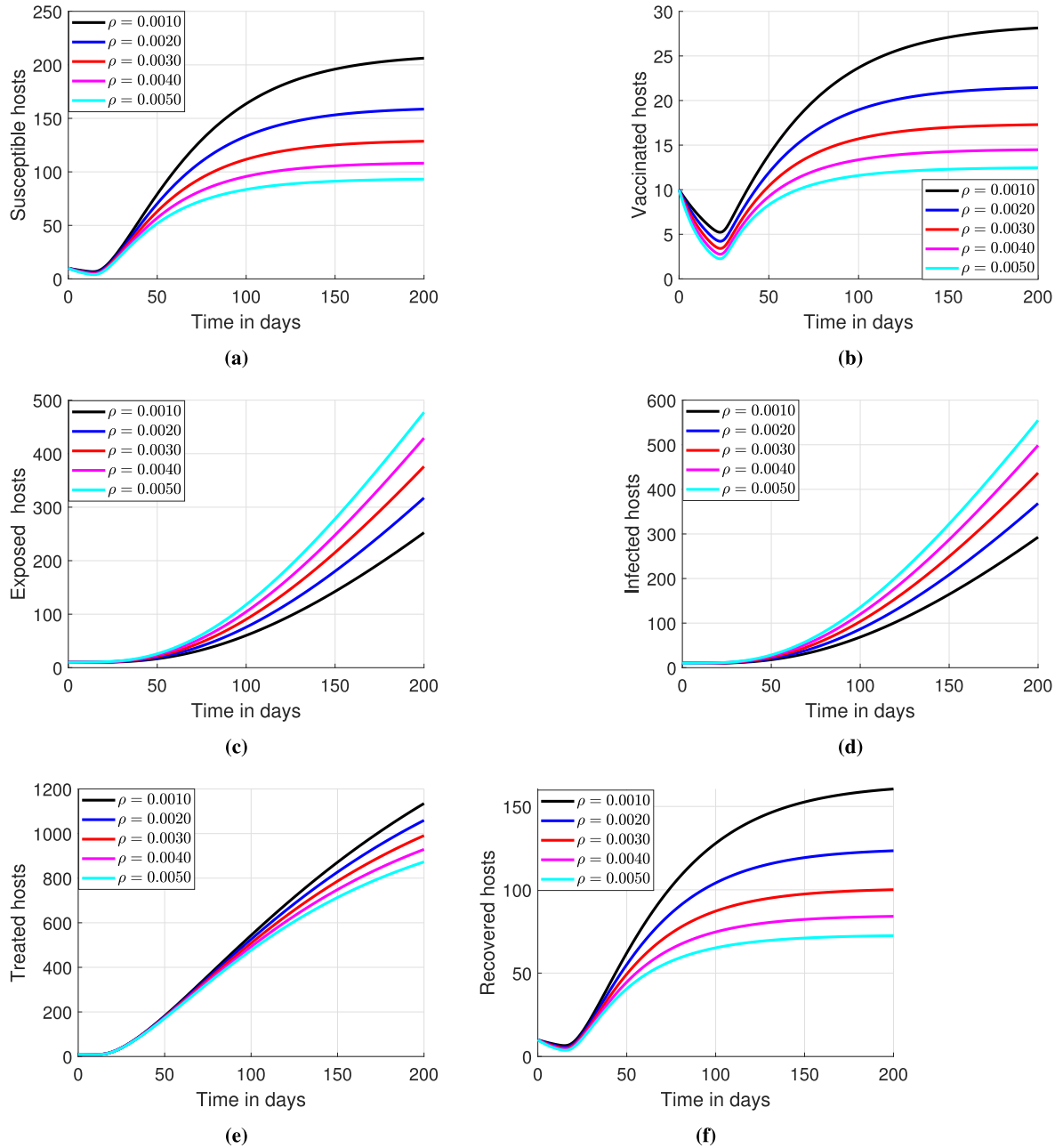


Fig. 7. Dynamics of the SVETIR population under varying ρ .

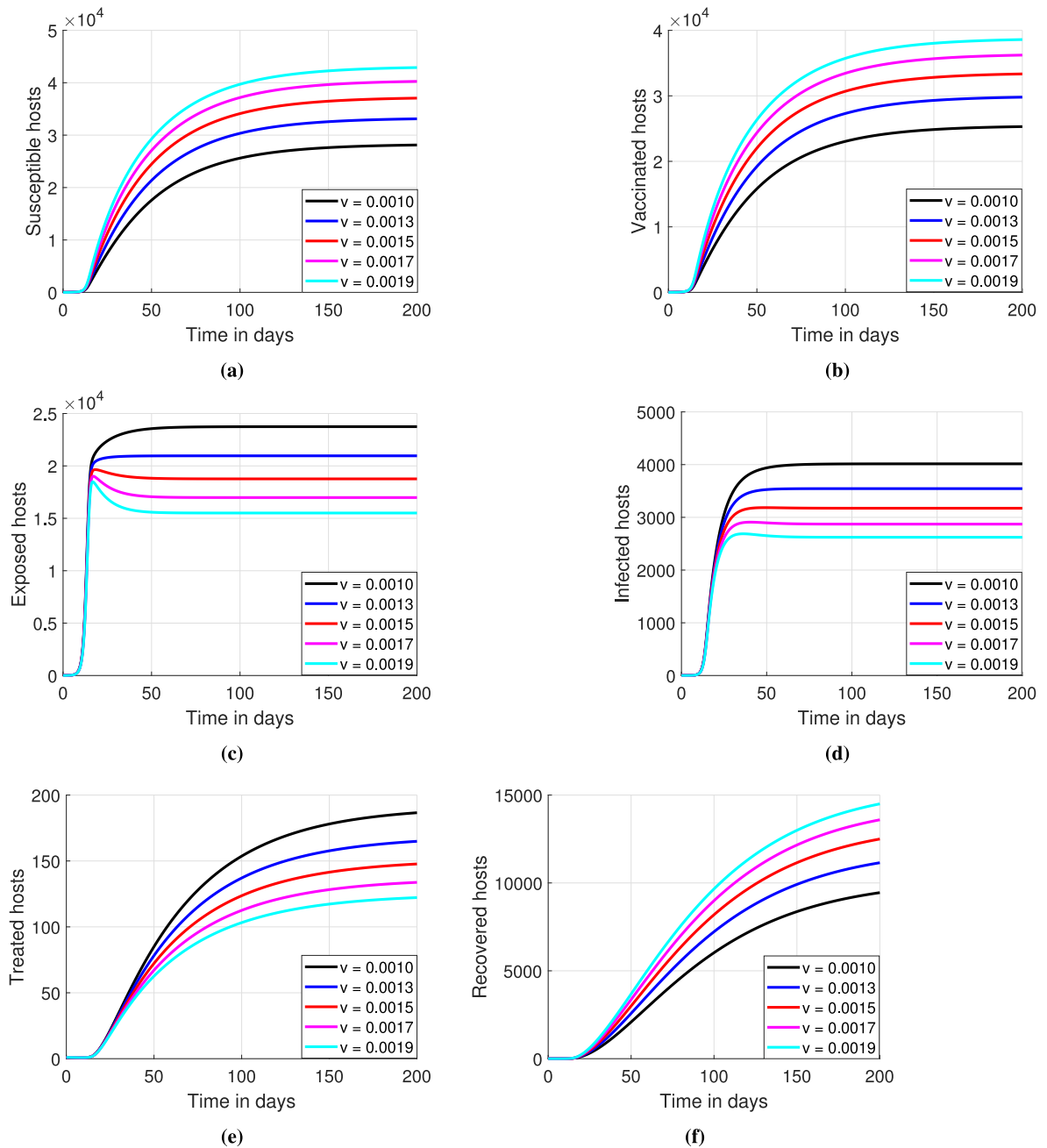


Fig. 8. Dynamics of the SVEITR population under varying v .

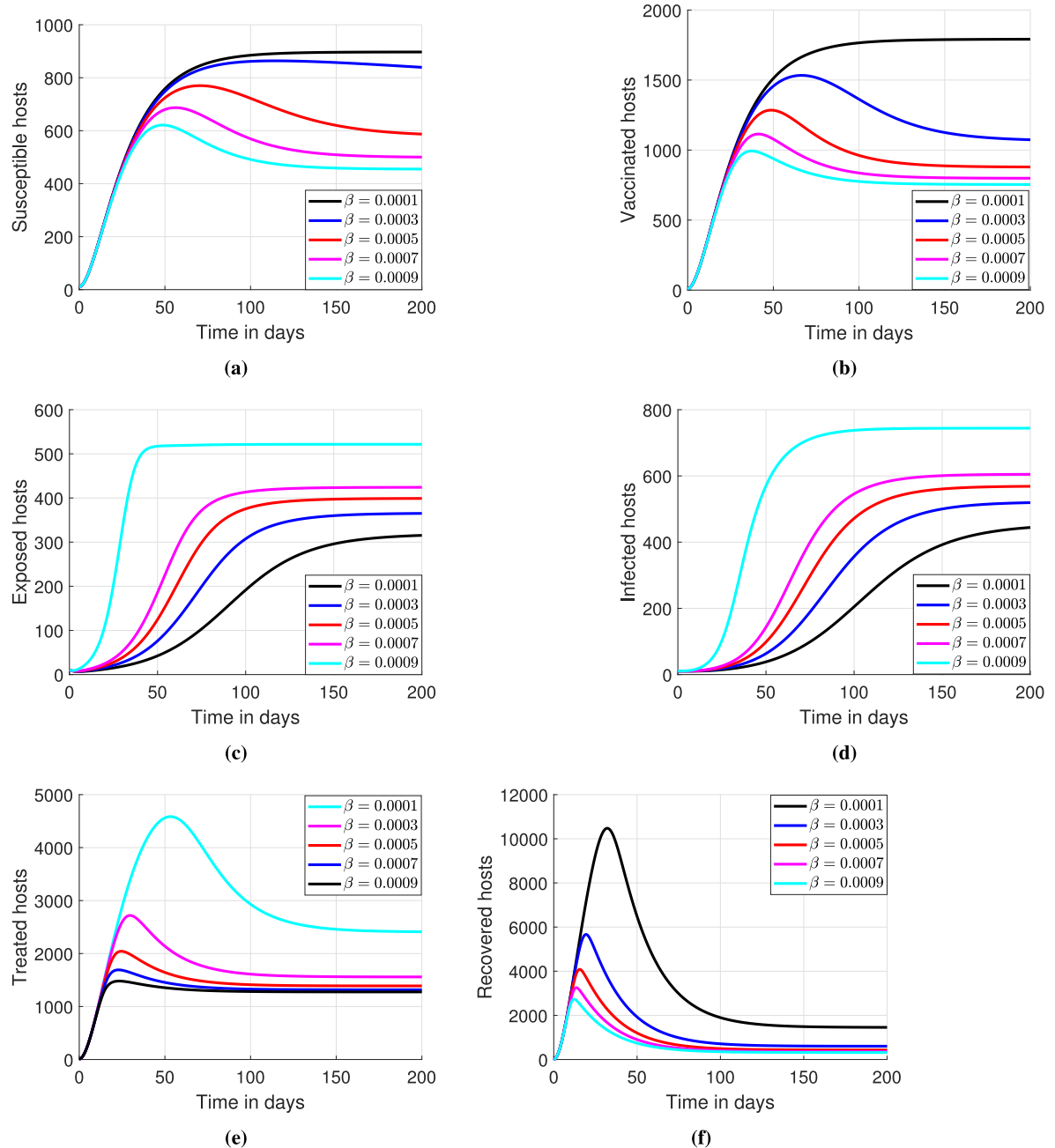


Fig. 9. Dynamics of the SVEITR population under varying β .

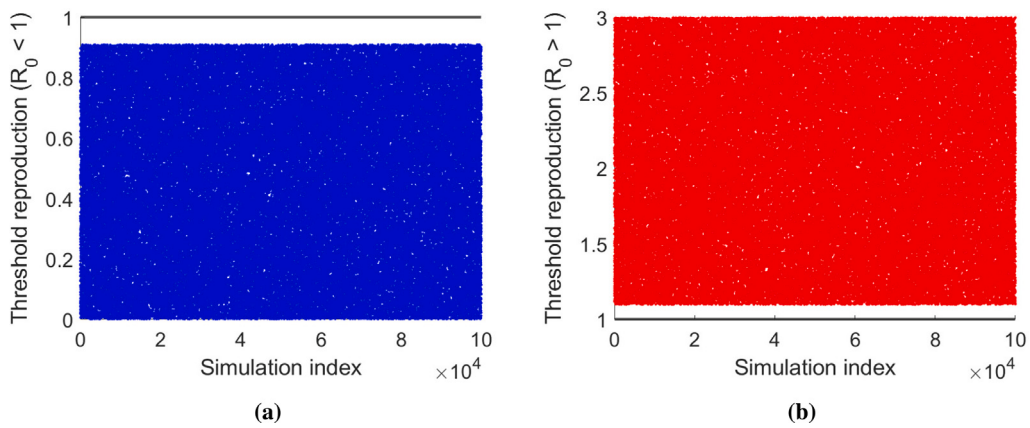


Fig. 10. Posterior simulations of the threshold reproduction R_0 .

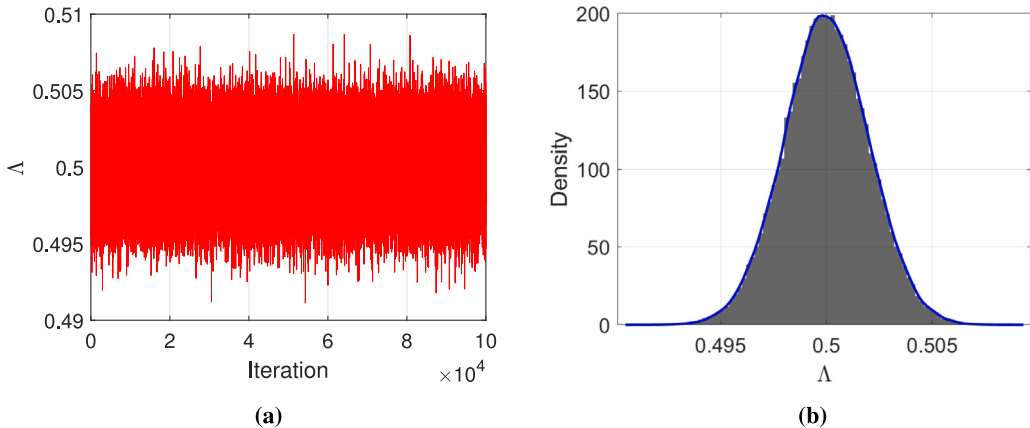


Fig. 11. Convergence of the susceptible influx parameter Λ .

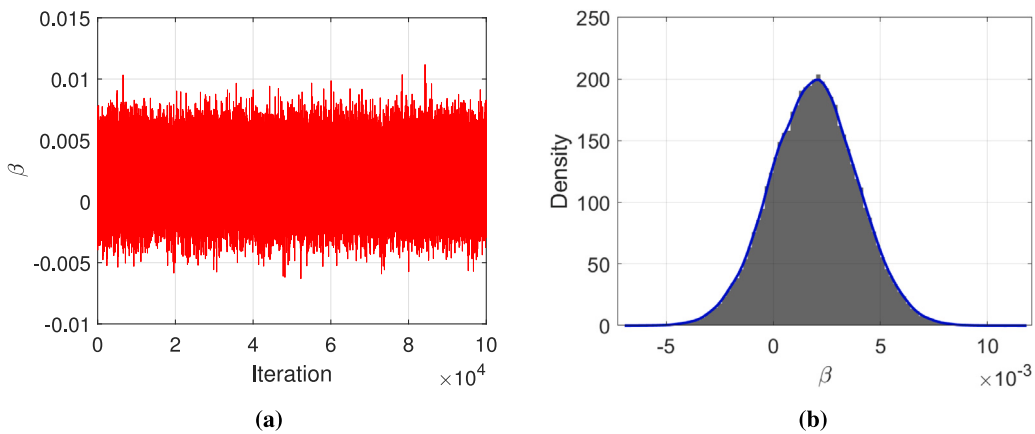


Fig. 12. Convergence diagnostics for the force-of-infection parameter β .

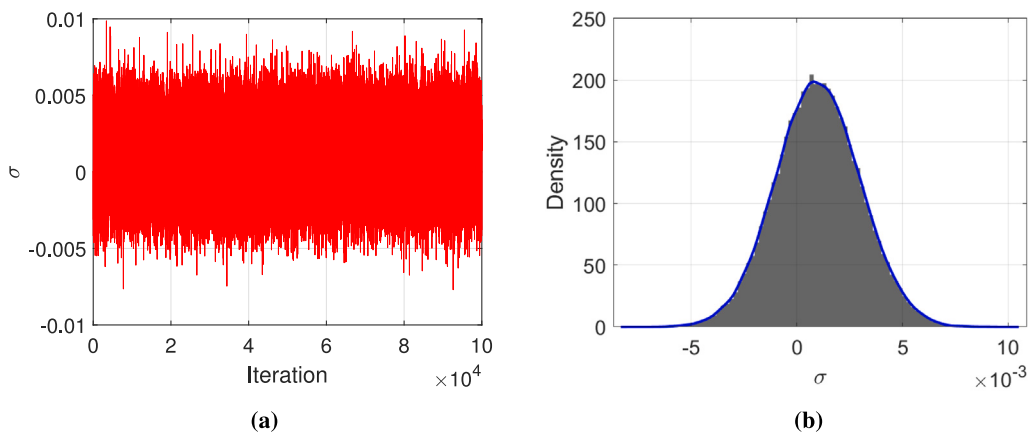


Fig. 13. Convergence diagnostics for the treatment parameter σ .

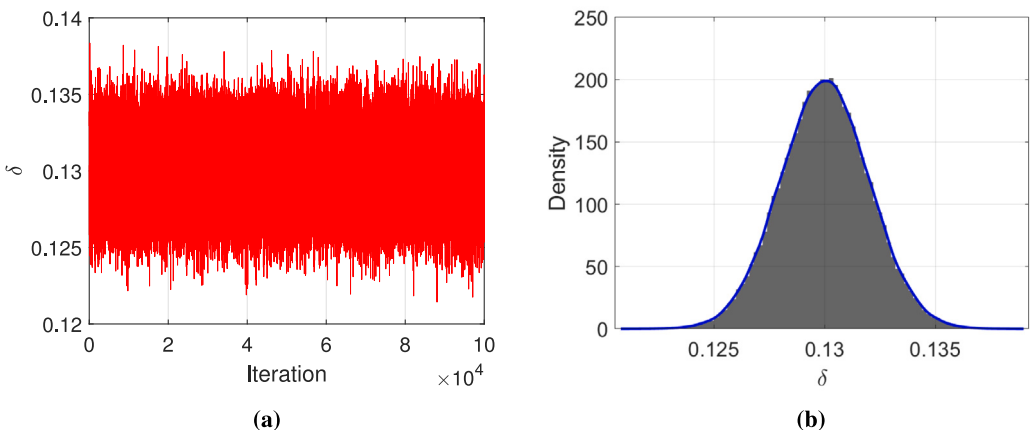


Fig. 14. Convergence diagnostics for the disease-induced parameter δ .

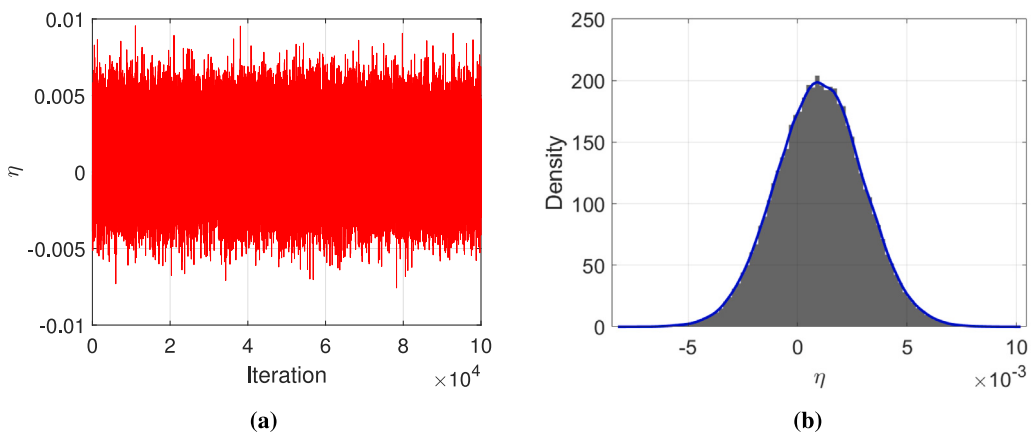


Fig. 15. Convergence diagnostics for the recovery-treatment parameter η .

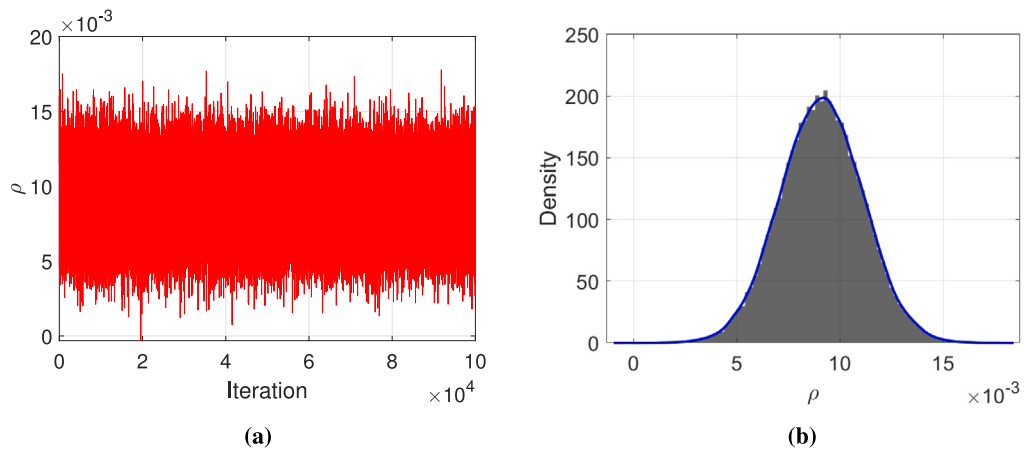


Fig. 16. Convergence diagnostics for the vaccination–susceptible parameter ρ .

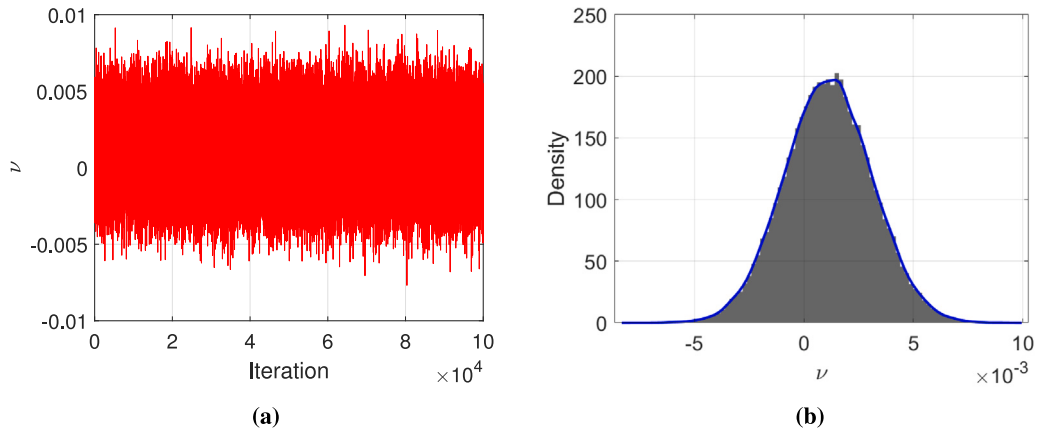


Fig. 17. Convergence diagnostics for the vaccination–exposed parameter ν .

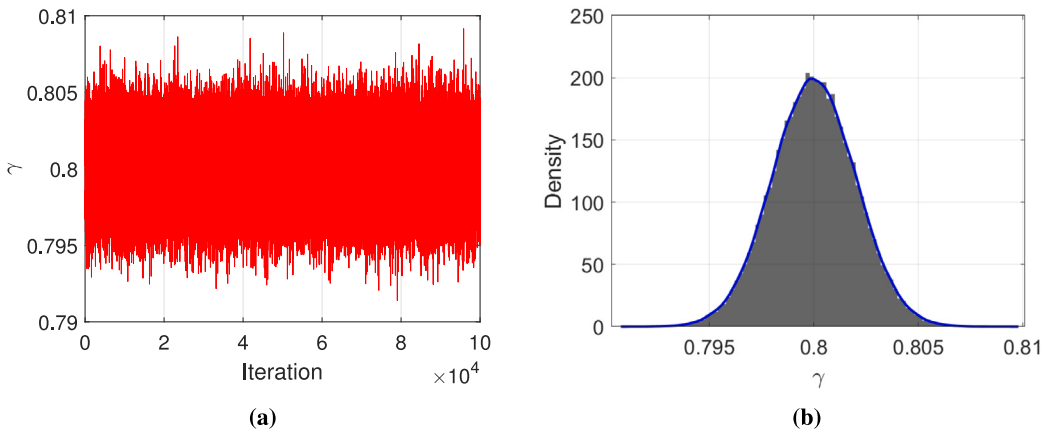


Fig. 18. Convergence diagnostics for the recovery–vaccinated parameter γ .

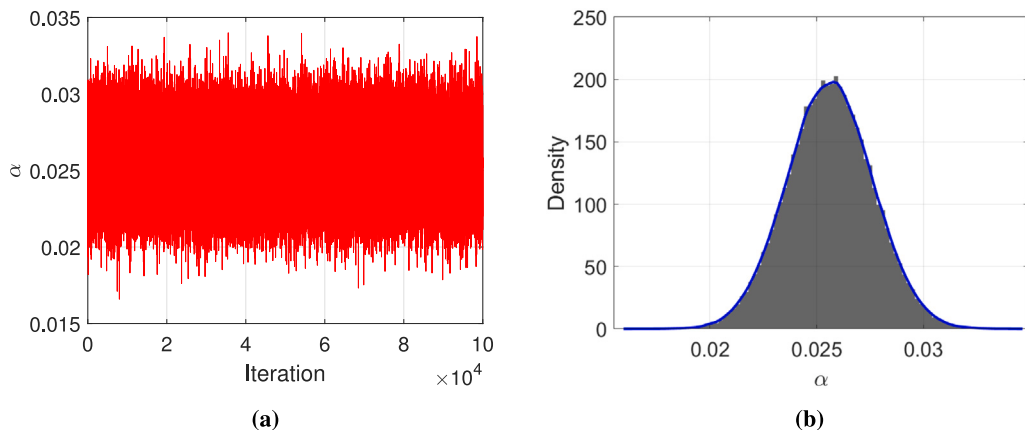


Fig. 19. Convergence diagnostics for the progression-from-exposed-to-infected parameter γ .

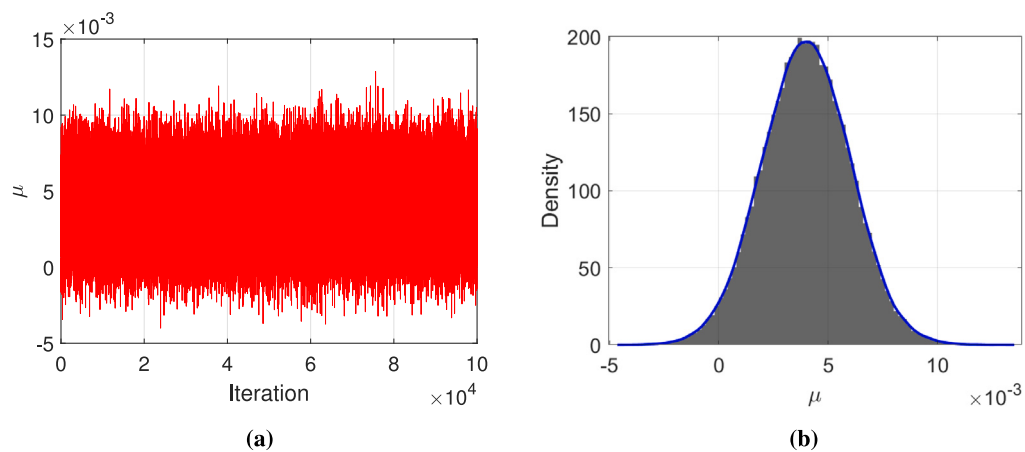


Fig. 20. Convergence diagnostics for the mortality rate parameter μ .

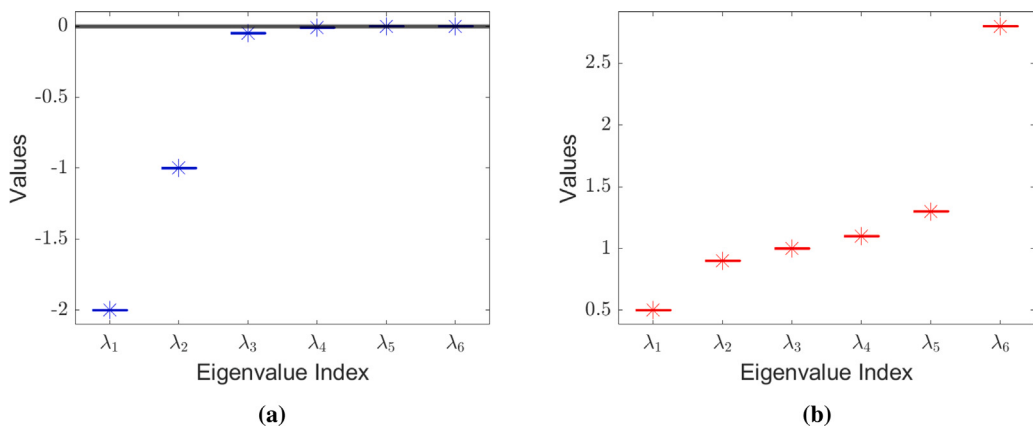


Fig. 21. Eigenvalue distributions for infection-free and persistent-infection point.

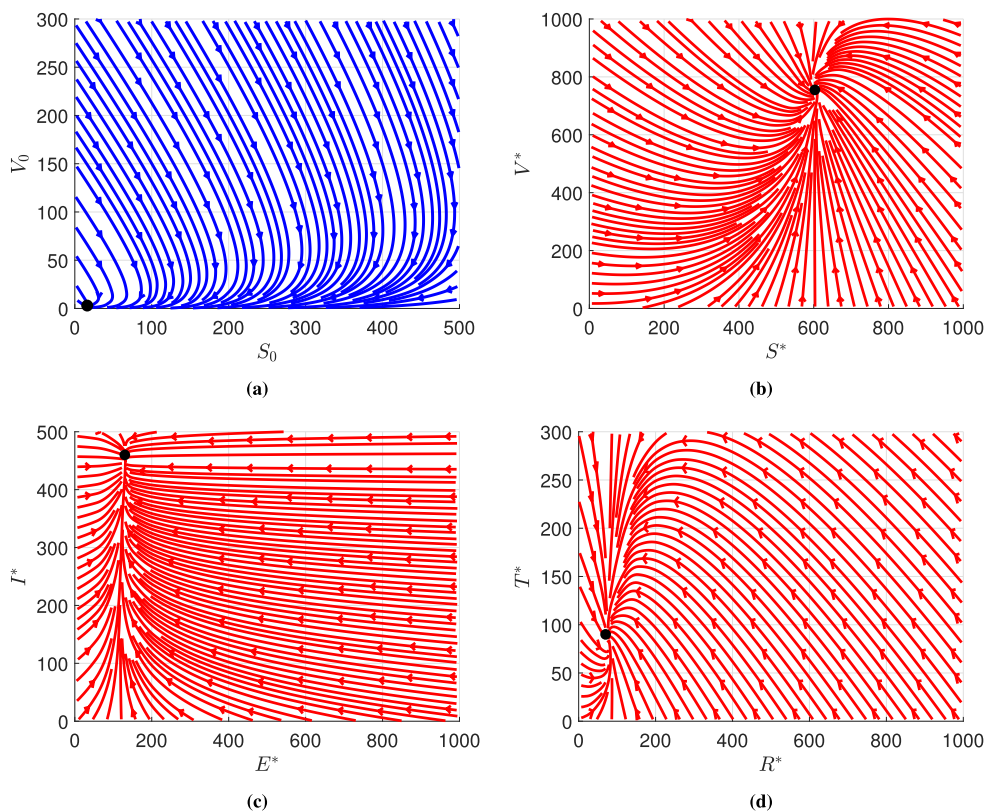


Fig. 22. Phase portrait showing convergence of equilibria.

Data availability

No data was used for the research described in the article.

References

- [1] World Health Organization. Measles. 2024, Available at: <https://www.who.int/health-topics/measles>.
- [2] Zhou Y, Su JM, Samuel CE, Ma D. Measles virus forms inclusion bodies with properties of liquid organelles. *J Virol* 2019;93. <http://dx.doi.org/10.1128/JVI.00948-19>.
- [3] Minta AA, Ferrari M, Antoni S, Lambert B, Sayi TS, Hsu CH, et al. Progress toward measles elimination — Worldwide, 2000–2023. *MMWR Morb Mortal Wkly Rep* 2024;73:1036–42. <http://dx.doi.org/10.15585/mmwr.mm7345a4>.
- [4] Atkinson W. Epidemiology and prevention of vaccine-preventable diseases. Department of Health & Human Services, Centers for Disease Control and Prevention; 2006, <https://stacks.cdc.gov/view/cdc/78725>.
- [5] Zumla A, Mandell, Douglas, and Bennett's principles and practice of infectious diseases. *Lancet Infect Dis* 2010;10:4–303. [http://dx.doi.org/10.1016/S1473-3099\(10\)70089-X](http://dx.doi.org/10.1016/S1473-3099(10)70089-X).
- [6] May T. Public communication, risk perception, and the viability of preventive vaccination against communicable diseases. *Bioethics* 2005;19:407–21. <http://dx.doi.org/10.1111/j.1467-8519.2005.00452.x>.
- [7] Lahariya C. Vaccine epidemiology: A review. *J Fam Med Prim Care* 2016;5:7. <http://dx.doi.org/10.4103/2249-4863.184616>.
- [8] Patel M, Lee AD, Clemons NS, Redd SB, Poser S, Blog D, et al. National update on measles cases and outbreaks — United States. 2019, n.d.
- [9] Battegaglia R, Itin C, Itin P. Dermatological signs and symptoms of measles: A prospective case series and comparison with the literature. *Dermatology* 2012;224:1–4. <http://dx.doi.org/10.1159/000335091>.
- [10] Bester JC. Measles and measles vaccination. *JAMA Pediatr* 2016;170:1209. <http://dx.doi.org/10.1001/jamapediatrics.2016.1787>.
- [11] Cutts FT, Ferrari MJ, Krause LK, Tatem AJ, Mosser JF. Vaccination strategies for measles control and elimination: time to strengthen local initiatives. *BMC Med* 2021;19:2. <http://dx.doi.org/10.1186/s12916-020-01843-z>.
- [12] Chilot D, Belay DG, Shitu K, Gela YY, Getnet M, Mulat B, et al. Measles second dose vaccine utilization and associated factors among children aged 24–35 months in Sub-Saharan Africa, a multi-level analysis from recent DHS surveys. *BMC Public Health* 2022;22:2070. <http://dx.doi.org/10.1186/s12889-022-14478-x>.
- [13] Sato R, Haraguchi M. Effect of measles prevalence and vaccination coverage on other disease burden: evidence of measles immune amnesia in 46 African countries. *Hum Vaccin Immunother* 2021;17:6–5361. <http://dx.doi.org/10.1080/21645515.2021.2013078>.
- [14] Kanchanarat S, Nuddee K, Chinviriyasit S, Chinviriyasit W. Mathematical analysis of pulse vaccination in controlling the dynamics of measles transmission. *Infect Dis Model* 2023;8:964–79. <http://dx.doi.org/10.1016/j.idm.2023.08.001>.

- [15] Cutts FT, Danovaro-Holliday MC, Rhoda DA. Challenges in measuring supplemental immunization activity coverage among measles zero-dose children. *Vaccine* 2021;39:1359–63. <http://dx.doi.org/10.1016/j.vaccine.2020.11.050>.
- [16] Kuddus MA, Mohiuddin M, Rahman A. Mathematical analysis of a measles transmission dynamics model in Bangladesh with double dose vaccination. *Sci Rep* 2021;11:16571. <http://dx.doi.org/10.1038/s41598-021-95913-8>.
- [17] Pasadyn F, Mamo N, Caplan A. Battling measles: Shifting strategies to meet emerging challenges and inequities. *Ethics Med Public Health* 2025;33:101047. <http://dx.doi.org/10.1016/j.jemep.2025.101047>.
- [18] De Serres G, Boulianne N, Defay F, Brousseau N, Benoît M, Lacoursière S, et al. Higher risk of measles when the first dose of a 2-dose schedule of measles vaccine is given at 12–14 months versus 15 months of age. *Clin Infect Dis* 2012;55:394–402. <http://dx.doi.org/10.1093/cid/cis439>.
- [19] Arsal SR, Aldila D, Handari BD. Short review of mathematical model of measles. 2020, 020003. <http://dx.doi.org/10.1063/5.0023439>.
- [20] Chatterjee AN, Sharma SK, Al Basir F A. A compartmental approach to modeling the measles disease: a fractional order optimal control model. *Fractal Fract* 2024;8:446. <http://dx.doi.org/10.3390/fractfract8080446>.
- [21] Abboubakar H, Fandio R, Sofack BS, Ekobena Fouada HP. Fractional dynamics of a measles epidemic model. *Axioms* 2022;11:363. <http://dx.doi.org/10.3390/axioms11080363>.
- [22] Brauer F, Castillo-Chavez C. In: *Mathematical models in population biology and epidemiology*, vol. 40, New York, NY: Springer New York; 2012. <http://dx.doi.org/10.1007/978-1-4614-1686-9>.
- [23] Qureshi S, Jan R. Modeling of measles epidemic with optimized fractional order under Caputo differential operator. *Chaos Solitons Fractals* 2021;145:110766. <http://dx.doi.org/10.1016/j.chaos.2021.110766>.
- [24] Lu C, Li L, Shah K, Abdalla B, Abdeljawad T. Mathematical insights into chaos in fractional-order fishery model. *Model Earth Syst Env* 2025;11:201. <http://dx.doi.org/10.1007/s40808-025-02375-2>.
- [25] Alemneh HT, Belay AM. Modelling, analysis, and simulation of measles disease transmission dynamics. *Discrete Dyn Nat Soc* 2023;1–20. <http://dx.doi.org/10.1155/2023/9353540>.
- [26] Mondaini RP, editor. *Trends in biomathematics: modeling epidemiological, neuronal, and social dynamics*. Cham: Springer Nature Switzerland; 2023.
- [27] Pang D, Wu X, Li C, Wang Z. Modeling and analysis of measles epidemic model with memory effect. *Int J Dyn Control* 2025;13:314. <http://dx.doi.org/10.1007/s40435-025-01824-1>.
- [28] Zakirullah. A mathematical model of pneumococcal pneumonia infection dynamics using treatment and vaccination interventions. *Int J Appl Comput Math* 2025;11:112. <http://dx.doi.org/10.1007/s40819-025-01928-4>.
- [29] Berhe HW, Makinde OD. Computational modelling and optimal control of measles epidemic in human population. *Biosystems* 2020;190:104102. <http://dx.doi.org/10.1016/j.biosystems.2020.104102>.
- [30] Rahmayani SA, Aldila D, Handari BD. Cost-effectiveness analysis on measles transmission with vaccination and treatment intervention. *AIMS Math* 2021;6:527–12491. <http://dx.doi.org/10.3934/math.2021271>.
- [31] Patel MK, Goodson JL, Alexander JP, Kretsinger K, Sodha SV, Steulet C, et al. Progress toward regional measles elimination — Worldwide, 2000–2019. *MMWR Morb Mortal Wkly Rep* 2020;69:5–1700. <http://dx.doi.org/10.15585/mmwr.mm6945a6>.
- [32] Gastañaduy PA, Banerjee E, DeBolt C, Bravo-Alcántara P, Samad SA, Pastor D, et al. Public health responses during measles outbreaks in elimination settings: Strategies and challenges. *Hum Vaccin Immunother* 2018;14:2222–38. <http://dx.doi.org/10.1080/21645515.2018.1474310>.
- [33] Islam MR, Peace A, Medina D, Oraby T. Integer versus fractional order SEIR deterministic and stochastic models of measles. *Int J Environ Res Public Health* 2020;17:2014. <http://dx.doi.org/10.3390/ijerph17062014>.
- [34] Sowole SO, Ibrahim A, Sangare D, Lukman AO. Mathematical model for measles disease with control on the susceptible and exposed compartments. *Open J Math Anal* 2020;4:60–75. <http://dx.doi.org/10.30538/psrp-oma2020.0053>.
- [35] Abo-Ezz ER, Essa KS. A least-squares minimization approach for model parameters estimate by using a new magnetic anomaly formula. *Pure Appl Geophys* 2016;173:1265–78. <http://dx.doi.org/10.1007/s00024-015-1168-9>.
- [36] Gibson G. Estimating parameters in stochastic compartmental models using Markov chain methods. *Math Med Biol* 1998;15:19–40. <http://dx.doi.org/10.1093/imammb/15.1.19>.
- [37] Li L, Shah K, Abdalla B, Abdeljawad T. Using treatment and vaccination strategies to investigate transmission dynamics of influenza mathematical model. *Ain Shams Eng J* 2025;16:103519. <http://dx.doi.org/10.1016/j.asen.2025.103519>.
- [38] Diekmann O, Heesterbeek JAP, Roberts MG. The construction of next-generation matrices for compartmental epidemic models. *J R Soc Interface* 2010;7:873–85. <http://dx.doi.org/10.1098/rsif.2009.0386>.
- [39] Dayan F, Ahmed N, Rafiq M, Raza A, Khan I, Eldin EMT. A reliable numerical investigation of an SEIR model of measles disease dynamics with fuzzy criteria. *Sci Rep* 2023;13:15840. <http://dx.doi.org/10.1038/s41598-023-42953-x>.
- [40] Gibson G. Estimating parameters in stochastic compartmental models using Markov chain methods. *Math Med Biol* 1998;15:19–40. <http://dx.doi.org/10.1093/imammb/15.1.19>.
- [41] Andrieu C, Thoms J. A tutorial on adaptive MCMC. *Stat Comput* 2008;18:343–73. <http://dx.doi.org/10.1007/s11222-008-9110-y>.
- [42] He J-H. Homotopy perturbation method: a new nonlinear analytical technique. *Appl Math Comput* 2003;135:9–73. [http://dx.doi.org/10.1016/S0096-3003\(01\)00312-5](http://dx.doi.org/10.1016/S0096-3003(01)00312-5).
- [43] Mechee MS, Al-Juaifri GA. Application of homotopy perturbation method for SIR model with vital dynamics and constant population. *Am J Appl Sci* 2018;15:10–21. <http://dx.doi.org/10.3844/ajassp.2018.10.21>.